CHALMERS
UNIVERSITY OF TECHNOLOGY

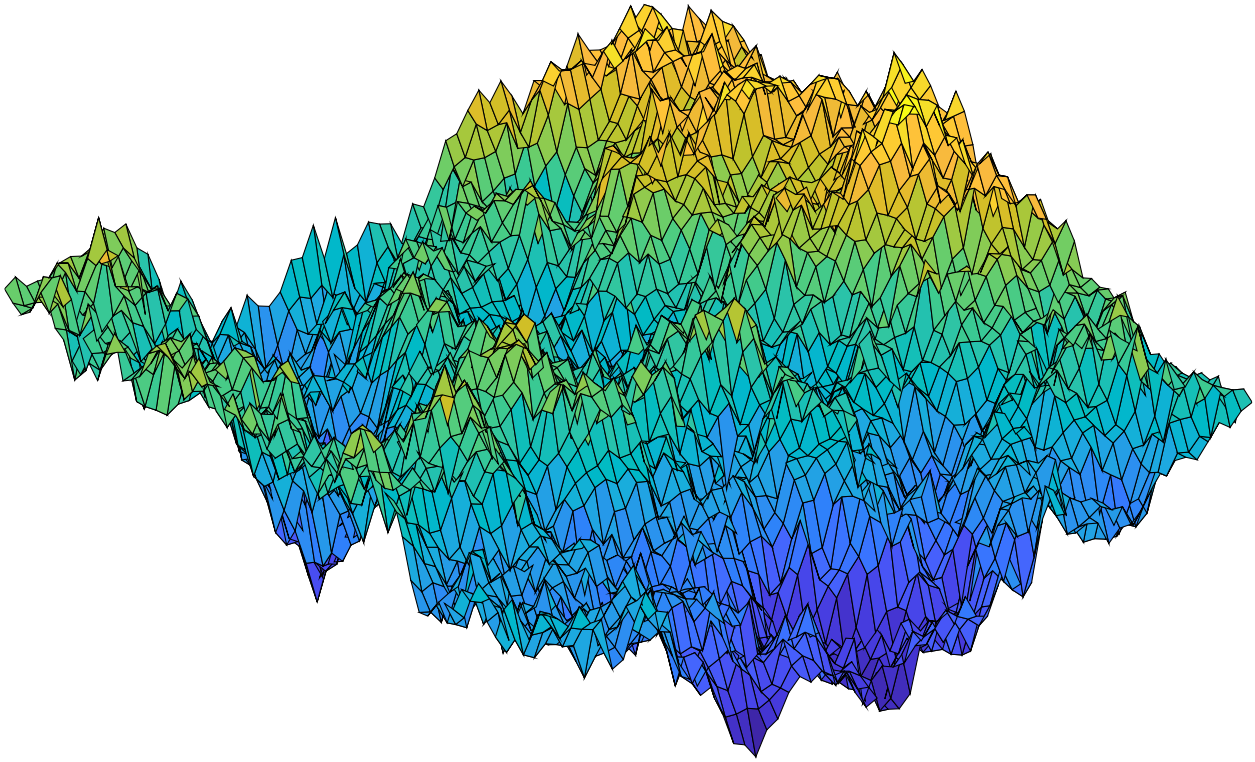

Approximation of non-stationary fractional Gaussian random fields

Master's thesis in Engineering Mathematics and Computational Science

Kasper Bågmark

Department of Mathematical Sciences
CHALMERS UNIVERSITY OF TECHNOLOGY
Gothenburg, Sweden 2020

Master's thesis 2020:NN

Approximation of non-stationary fractional Gaussian random fields

Kasper Bågmark

CHALMERS
UNIVERSITY OF TECHNOLOGY

Mathematical Sciences
Chalmers University of Technology
Gothenburg, Sweden 2020

Approximation of non-stationary fractional Gaussian random fields
Kasper Bågmark

Supervisor: Annika Lang, Mathematical Sciences
Examiner: Annika Lang, Mathematical Sciences

Master's Thesis 2020:NN
Mathematical Sciences
Chalmers University of Technology
SE-412 96 Gothenburg
Telephone +46 31 772 1000

Cover: A fractional Brownian motion with Hurst index $H = 0.4$.

Typeset in LaTeX
Printed by Chalmers Reproservice
Gothenburg, Sweden 2020

Approximation of non-stationary fractional Gaussian random fields
Kasper Bågmark
Mathematical Sciences
Chalmers University of Technology

Abstract

Numerical approximations of fractional and multifractional Brownian fields are studied by measuring the numerical convergence order. In order to construct these non-stationary fields a study of Gaussian fields, fractal analysis and self-similarity is conducted. The random fields are defined through their covariance function. Simulations are constructed through the Cholesky method, which builds on the Cholesky decomposition of the covariance matrix in order to accurately simulate the non-stationary field. The strong error in $L^2(\Omega; L^2(T; \mathbb{R}))$ is measured for the fractional Brownian motion defined by the fixed Hurst parameter H. It is shown numerically that the convergence rate α satisfies $\alpha > H$ for $H \in (0, 0.6)$. Furthermore the convergence rates are measured for multifractional Brownian motions defined by Hurst functions $h : T \to (0, 1)$ of varying form.

Keywords: Multifractional Brownian motion, non-stationary random fields, Cholesky method, numerical strong convergence rate

Acknowledgements

The first person I want to thank is my resourceful supervisor Annika Lang who has supported me tirelessly with feedback and insightful tips to my thesis during this last year. I also want to thank Tomas Forssmark and Oskar Eklund for valuable input to my implementations and numerical modelling. I am grateful to Adam Östberg, David Ericsson, Simon Johansson and Emma Darebro who helped me take my mind of my thesis at times. Finally I want to thank my partner Ellen for her immense support and putting up with me during intense periods.

Kasper Bågmark, Gothenburg, May 2020

Contents

List of Figures

1

Introduction

The study of numerical approximations has been an area with enormous growth in the last decades. This accounts for both the methods developed but perhaps even more the actual implementations that now can be assessed in a reasonable fashion. It is now possible to examine how efficient a method is to numerically approximate its target, for example by evaluating the order of convergence for the method. In this thesis we will study the approximation of non-stationary fractional Gaussian random fields. What this comes down to is essentially twofold. First, we consider fractional fields, a fundamental example is the fractional Brownian motion. Commonly denoted B_H the fractional Brownian motion is an extension to the famous Brownian motion for which $H = 1/2$. This $H \in (0, 1)$ denotes the Hurst parameter, or Hölder-exponent, of the process and directly dictates the fractal dimension of the process to be $2 - H$. Secondly we consider this non-stationarity by letting the Hurst parameter H vary over the domain and hence we lose the stationarity of the increments of the field.

Fractional Brownian motion was rigorously defined by the "fractalist" Mandelbrot in 1968 but had already been implicitly used earlier, e.g. Kolmogorov [13]. Mandelbrot examined multiple fractal geometries in his days, both from a theoretical framework but also physical phenomenon [14],[15]. One of the many contributions from Mandelbrot was regarding self-similarity. Fractional Brownian motion exhibits this property and is one of the reasons this process has many applications in finance, telecommunication, physical phenomenon and medicine.

One such application is covered in [17] where it is explained how multifractal analysis is used to analyze X-ray images of breast tissue. This is used when looking for anomalies that could be early stages of breast cancer. The tissue does exhibit self-similarity with regard to a local Hurst parameter and then the anomalies can be found by looking for irregularities of the Hurst parameter in local patches.

Multifractional Brownian fields are the generalization of fractional Brownian fields which consider a Hurst parameter $H \in (0, 1)$ that can vary in the domain. We define this by a function $h : T \to (0, 1)$ where $T \subset \mathbb{R}^d$. The theoretical background of this family of fields is explained and thoroughly defined in [4]. In this thesis we want to extend their study and numerically investigate methods of approximation that are presented in their final chapter. We will thus consider their framework and adapt to

a setting with an implementation such that we can construct methods of measuring the numerical convergence.

For this purpose we will consider the Cholesky method, based on Cholesky decomposition since this is an exact method and thus appropriate to measure the strong convergence rate of a field. Although other methods have been shown to generate fields with a high accuracy [3], these methods deem not appropriate for a numerical convergence study which this thesis aims to handle. Based on the covariance function of a centered multifractional Brownian motion,

$$\mathbb{E}\left[B_h(x)B_h(y)\right] = D(h(x),h(y))\left(\|x\|^{h(x)+h(y)} + \|y\|^{h(x)+h(y)} - \|x-y\|^{h(x)+h(y)}\right) \tag{1.1}$$

where

$$D(s,t) = \frac{\sqrt{\Gamma(2s+1)\Gamma(2t+1)\sin(\pi s)\sin(\pi t)}\Gamma(\frac{s+t+1}{2})}{2\Gamma(s+t+1)\sin(\pi(s+t))\Gamma(\frac{s+t+d}{2})}, \tag{1.2}$$

we can construct a covariance matrix on the discretized domain V^h which is vital to the Cholesky method.

Although we do not show any analytical results of the convergence order, we are successful in showing a linear relation between the Hurst parameter of a fractional Brownian motion and the order of convergence. That is, for $H \in (0, 0.6)$ we can show that $\alpha > H$, where α is the order of the strong convergence. The error is measured in the space of $L^2(\Omega; L^2(T;\mathbb{R}))$ and is defined as

$$\mathbb{E}\left[\left\|X - \widehat{X_h}\right\|^2_{L^2(T)}\right]^{1/2} = \mathbb{E}\left[\int_T |X(t) - \widehat{X_h}(t)|^2 \,\mathrm{d}t\right]^{1/2}, \tag{1.3}$$

where $T = [0,1]$. This domain accurately catches the properties of the process since it is a self-similar process. Furthermore we measure the convergence of multifractional Brownian motions defined by different functions h that define the process. For these we obtain higher convergence order than before, primarily for processes that are defined by a strictly increasing Hurst parameter.

This thesis is divided into three parts that aim to cover the theoretical background, the approximation and finally the numerical convergence. In Chapter 2, we cover the basics of stochastic analysis where we generalize the concept of stochastic processes to higher dimensions. We emphasize on the properties of Gaussian fields and stationarity before defining the Hausdorff dimension. To finally define fractional Brownian field we explain the concept of self-similarity and then illustrate example paths of these fields. In the last part we define multifractional Brownian fields which concludes the theoretical framework.

Chapter 3 covers the approximation of the fields. We explain and define the strong convergence, how this is discretized and adjusted to a Monte Carlo sampling. Although the Cholesky method is the one opted for we make arguments why and what

the obvious drawbacks of this decision are. Other methods mentioned include the random midpoint displacement and the FieldSim algorithm which both are defined and why they deem unsuitable for this study. Finally the chapter concludes with the implemented algorithm to measure the strong error.

In Chapter 4 we present the numerical results of the convergence study. We start by recalling the examples of the fractional Brownian motion and evaluate the order of convergence of these processes. Next, we investigate the convergence order of a fBm defined by all $H \in (0, 1)$. Furthermore, we evaluate the convergence for multifractional Brownian motion. We consider different sorts of Hurst functions: increasing, decreasing, sinusoids and discontinuous. The corresponding convergence rates are measured for all of these and are illustrated with a short discussion about their relation to the Hurst function h.

2

Theory

The general idea when constructing a Gaussian field is to consider the covariance function of the field. This chapter will aim to show and explain the concepts and definitions that are required to define the covariance function of a multifractional Brownian field. As we progress further into the theory we will present examples of explicit processes and fields that will follow us through the rest of this thesis. The reader is assumed to possess some general knowledge regarding probability distributions, measure theory and functional analysis.

Section-wise we will begin by defining the generalization of stochastic processes to a general dimension d. In the second section we briefly relate how fractals and the Hausdorff dimension relate to the Hurst exponent. Finally in the third and fourth section we will define fractional Brownian fields and multifractional Brownian fields, respectively. Most of this chapter is covered in [4] and hence a more detailed background can be found there.

2.1 Stochastic fields

This first section covers the basics of stochastic fields, which particular includes the Gaussian distribution and the property of stationarity which is stressed. Here we will early present the famous Brownian motion as one of the important examples. The section is divided into four parts: definitions, Gaussian fields, Gaussian random measure and stationary fields.

2.1.1 Definitions

Definition 2.1.1. Let T be a set and $(E, \mathcal{E})$ a measurable space. A *stochastic field* $(X(t),\ t \in T)$ taking values in $(E, \mathcal{E})$ is a collection of measurable maps $X(t)$ from a probability space $(\Omega, \mathcal{A}, \mathbb{P})$ to $(E, \mathcal{E})$.

In the context of this report T will be $\mathbb{R}^d$ or a subset thereof and approximation-wise $d = 1, 2$ will be used. The measurable space $(E, \mathcal{E})$ will be $(\mathbb{R}, \mathcal{B}(\mathbb{R}))$, where $\mathcal{B}$ denotes the Borel σ-algebra. If the domain T is of one dimension we call X a *stochastic process*.

Definition 2.1.2. The *finite dimensional distributions* of a stochastic field $(X(t),\ t \in T)$ are defined by the random vector $(X(t_1), \ldots, X(t_n))$ for every $n \geq 1$ and $t_1, \ldots, t_n \in$

T. Two stochastic fields are said to be *versions* of each other if they have the same finite dimensional distributions for each n and $(t_1, \ldots, t_n) \in T^n$.

These distributions are relevant in understanding a stochastic field. However, primarily it is through its characteristic function.

Definition 2.1.3. Let $(X(t),\ t \in T)$ be a stochastic field. The distribution of the random vector $(X(t_1), \ldots, X(t_n)),\ n \geq 1,\ (t_1, \ldots, t_n) \in T^n$ is represented by its *characteristic function* φ. It is defined for $(\lambda_1, \ldots, \lambda_n) \in \mathbb{R}^n$ as

$$\varphi_{t_1,\ldots,t_n}(\lambda_1, \ldots, \lambda_n) = \mathbb{E}\left[\exp\left(i\sum_{j=1}^{n} \lambda_j X(t_j)\right)\right].$$

An important theorem that ensures the existence of a stochastic field given a collection of consistent characteristic functions is Kolmogorov's consistency theorem.

Theorem 2.1.1 (Kolmogorov's consistency theorem)**.** *Let $(\varphi_{t_1,\ldots,t_n},\ n \geq 1,\ (t_1, \ldots, t_n) \in T^n)$ be a collection of characteristic functions. Now if for any permutation $(\sigma(1), \ldots, \sigma(n))$ of $(1, \ldots, n)$ and for $m \leq n$ the following two conditions are fulfilled*

$$\varphi_{t_1,\ldots,t_n}(\lambda_1, \ldots, \lambda_n) = \varphi_{t_{\sigma(1)},\ldots,t_{\sigma(n)}}(\lambda_{\sigma(1)}, \ldots, \lambda_{\sigma(n)}),$$
$$\varphi_{t_1,\ldots,t_m}(\lambda_1, \ldots, \lambda_m) = \varphi_{t_1,\ldots,t_n}(\lambda_1, \ldots, \lambda_m, 0, \ldots, 0),$$

then the finite dimensional distributions associated to these characteristic functions are called consistent. If the collection of characteristic functions is consistent then there exists a stochastic field $(X(t),\ t \in T)$ s.t. for any $n \geq 1$, $(t_1, \ldots, t_n) \in T^n$,

$$\varphi_{t_1,\ldots,t_n}(\lambda_1, \ldots, \lambda_n) = \mathbb{E}\left[\exp\left(i\sum_{j=1}^{n} \lambda_j X(t_j)\right)\right].$$

Definition 2.1.4. Let $(X(t),\ t \in T)$ be a stochastic field s.t. $\mathbb{E}\left[|X(t)|^2\right] < \infty,\ t \in T$. The mean value of X is then the function $t \mapsto m(t) = \mathbb{E}\left[X(t)\right]$. If $m(t) = 0$ for all $t \in T$ then the field is called a *centered field*. The *covariance function* is defined as the function $R : T \times T \to \mathbb{R}$

$$(t, s) \mapsto R(t, s) = \mathbb{E}\left[(X(t) - m(t))(X(s) - m(s))\right].$$

With the definition of the covariance function in mind we want to consider what sort of functions that are a covariance function, and reverse, which properties a covariance function must have.

Definition 2.1.5. A symmetric function $\psi : T \times T \to \mathbb{R} : (t, s) \mapsto \psi(t, s)$ is a *non-negative definite* function if for every $n \geq 1$, $(\lambda_1, \ldots, \lambda_n) \in \mathbb{R}^n$, $(t_1, \ldots, t_n) \in T^n$ it holds that

$$\sum_{i,j=1}^{n} \lambda_i \lambda_j \psi(t_i, t_j) \geq 0.$$

Proposition 2.1.1. *Let ψ be a non-negative definite function. Then for all $t, s \in T$, it holds that*

$$\psi(t,t) \geq 0,$$
$$\psi(t,t)\psi(s,s) \geq \psi(t,s)^2.$$

Proposition 2.1.2. *The covariance function $R : T \times T \to \mathbb{R}$ of a stochastic field is a non-negative definite function.*

Next we give a definition of non-negative definite with regard to the distance between two elements in T.

Definition 2.1.6. A function $f : T \to \mathbb{R}$ is called *non-negative definite* if the function $(t,s) \mapsto f(t-s)$ is non-negative definite in the sense of the previous definition. More precisely this converts to that for every $n \geq 1$, $(\lambda_1, \ldots, \lambda_n) \in \mathbb{R}^n$, $(t_1, \ldots, t_n) \in T^n$ it holds that

$$\sum_{i,j=1}^{n} \lambda_i \lambda_j f(t_i - t_j) \geq 0$$
$$f(-t) = f(t).$$

Theorem 2.1.2 (Bochner's theorem)**.** *Among the continuous real valued functions, the non-negative definite functions on $T = \mathbb{R}^d$ are those functions which are the Fourier transforms of finite symmetric measures.*

Definition 2.1.7. A real valued symmetric function $(t,s) \mapsto \phi(t,s)$ with $s,t \in T$, is a function of *negative* type if for every $n \geq 1$, $(\lambda_1, \ldots, \lambda_n) \in \mathbb{R}^n$ s.t. $\sum_{i=1}^{n} \lambda_i = 0$, $(t_1, \ldots, t_n) \in T^n$ it holds that

$$\sum_{i,j=1}^{n} \lambda_i \lambda_j \phi(t_i, t_j) \leq 0.$$

Theorem 2.1.3 (Schoenberg's theorem)**.** *Let $(t,s) \mapsto \phi(t,s)$, $s,t \in T$, be a real valued symmetric continuous function with $\phi(t,t) = 0$.*

1. *Fix $t_0 \in T$. Define ψ by*

$$\psi(t,s) = \phi(t_0,t) + \phi(t_0,s) - \phi(t,s)$$
$$\psi(s,t) = \phi(t_0,s) + \phi(t_0,t) - \phi(s,t) = \psi(t,s).$$

   Then ϕ is a function of negative type if and only if ψ is a real valued non-negative definite function.

2. *ϕ is a function of negative type if and only if $e^{-\lambda\phi}$ is a non-negative definite function for all $\lambda \geq 0$.*

This theorem yields an important corollary which will be relevant later with regard to the Hurst exponent.

Corollary 2.1.1.

- *Functions* $(t,s) \mapsto \|t\|^{2H} + \|s\|^{2H} - \|t-s\|^{2H}$, $t,s \in \mathbb{R}^n$ *are non-negative definite functions if and only if* $0 < H \leq 1$.
- *Functions* $t \mapsto e^{-|t|^\alpha}$, $t \in \mathbb{R}$ *are characteristic functions if and only if* $0 < \alpha \leq 2$.

Following the proof of [4] we show this vital property.

Proof. First we note that the mapping $(t,s) \mapsto \|t-s\|^2$ is of negative type, that is take $\sum_i^n \lambda_i = 0$.

$$\begin{aligned}
\sum_{i,j=1}^{n} \lambda_i \lambda_j \|t_i - t_j\|^2 &= \sum_{i,j=1}^{n} \lambda_i \lambda_j \left(\|t_i\|^2 + \|t_j\|^2 - 2\langle t_i, t_j \rangle \right) \\
&= \underbrace{\sum_{j=1}^{n} \lambda_j}_{=0} \sum_{i=1}^{n} \lambda_i \|t_i\|^2 + \underbrace{\sum_{i=1}^{n} \lambda_i}_{=0} \sum_{j=1}^{n} \lambda_j \|t_j\|^2 - 2 \sum_{i,j=1}^{n} \langle \lambda_i t_i, \lambda_j t_j \rangle \\
&= -2 \left\langle \sum_{i=1}^{n} \lambda_i t_i, \sum_{j=1}^{n} \lambda_j t_j \right\rangle \\
&= -2 \left\| \sum_{i=1}^{n} \lambda_i t_i \right\|^2 \leq 0.
\end{aligned}$$

By applying the first part of Schoenberg's theorem 2.1.3 with $t_0 = 0$ we have shown the case with $H = 1$. Next we use the following property which holds for $0 < H < 1$ and non-negative x,

$$x^H = C_H \int_0^\infty \frac{e^{-\lambda x} - 1}{\lambda^{1+H}} \, \mathrm{d}\lambda.$$

We can find $C_H^{-1} \neq 0$ and show that this holds by change of variables, $u = \lambda x$

$$\begin{aligned}
C_H \int_0^\infty \frac{e^{-\lambda x} - 1}{\lambda^{1+H}} \, \mathrm{d}\lambda &= C_H \int_0^\infty \frac{e^{-u} - 1}{\left(\frac{u}{x}\right)^{1+H}} \frac{\mathrm{d}u}{x} \\
&= C_H x^H \int_0^\infty \frac{e^{-u} - 1}{u^{1+H}} \, \mathrm{d}u,
\end{aligned}$$

which in turn implies that if we set

$$C_H^{-1} = \int_0^\infty \frac{e^{-u} - 1}{u^{1+H}} \, \mathrm{d}u,$$

we are done. Now inserting this into the previous function we get the modified version

$$\sum_{i,j=1}^{n} \lambda_i \lambda_j \|t_i - t_j\|^{2H} = C_H \int_0^\infty \frac{\sum_{i,j=1}^{n} \lambda_i \lambda_j e^{-\lambda \|t_i - t_j\|^2}}{\lambda^{1+H}} \, \mathrm{d}\lambda.$$

Next we apply the second part of Schoenberg's theorem 2.1.3.2, which says that $\sum_{i,j=1}^{n} \lambda_i \lambda_j e^{-\lambda \|t_i - t_j\|^2}$ is non-negative definite since $\|t_i - t_j\|^2$ is of negative type. However since $C_H < 0$ we have that the mapping $(t, s) \to \|t - s\|^{2H}$ is of negative type for $0 < H < 1$. Now it is easy to verify with the first part of Schoenberg's theorem 2.1.3.1 that the function $(t, s) \to \|t\|^{2H} + \|s\|^{2H} - \|t - s\|^{2H}$ is a non-negative definite function by inserting $t_0 = 0$.

To show that $H > 1$ cannot hold we provide a simple example with three points in $\mathbb{R}$ s.t. $|t_3 - t_2| = |t_2 - t_1| = 1$ and $|t_3 - t_1| = 2$. Let $\lambda_1 = \lambda_3 = -1$ and $\lambda_2 = 2$ then

$$\sum_{i,j=1}^{3} \lambda_i \lambda_j |t_i - t_j|^{2H} = -8 + 2^{2H+1} > 0$$

thus not of negative type and hence we are done. □

2.1.2 Gaussian fields

This part covers Gaussian distributed fields and brings light to some of their unique properties.

Definition 2.1.8. A random vector $X = (X_1, \ldots, X_d)$ is called a *Gaussian random vector* if any finite linear combination of its coordinates $\sum_{j=1}^{d} \lambda_j X_j,\ \lambda_j \in \mathbb{R}$ is a Gaussian random variable.

Definition 2.1.9. A random field Y is a *modification* of X if for every $t \in T$, $\mathbb{P}(X(t) = Y(t)) = 1$.

Definition 2.1.10. A process $(B(t))_{t \geq 0}$ satisfying the following conditions

1. $B(0) = 0$,
2. B has a modification $\tilde{B}$ that has almost surely continuous trajectories,
3. for all $s \leq t,$ the increment $B(t) - B(s)$ is independent of $(B(u),\ u \leq s)$,
4. $B(t) - B(s) \sim \mathcal{N}(0, |t - s|)$

is called a *standard Brownian motion.*

Example 2.1.1. In Figure 2.1 we have simulated a sample path of the standard Brownian motion on the domain $[0, 1]$ and at a later stage we will evaluate the convergence rate of this process given a numerical scheme. We will later come to see that this is just a special case of the more general fractional Brownian motion. The covariance function of the Brownian motion satisfies $R(t, s) = \mathbb{E}[B(t)B(s)] = \min(t, s)$.

Definition 2.1.11. A stochastic field $(X(t), t \in T)$ is a *Gaussian field*, if and only if, for all $n \geq 1$, $(t_1, \ldots, t_n) \in T^n$, the random vector $(X(t_1), \ldots, X(t_n))$ is a Gaussian random vector.

Theorem 2.1.4. *Let $m : T \to \mathbb{R}$ be a function and $R : T \times T \to \mathbb{R}$ be a non-negative definite function. If a stochastic field $(X(t), t \in T)$ satisfies the following equality,*

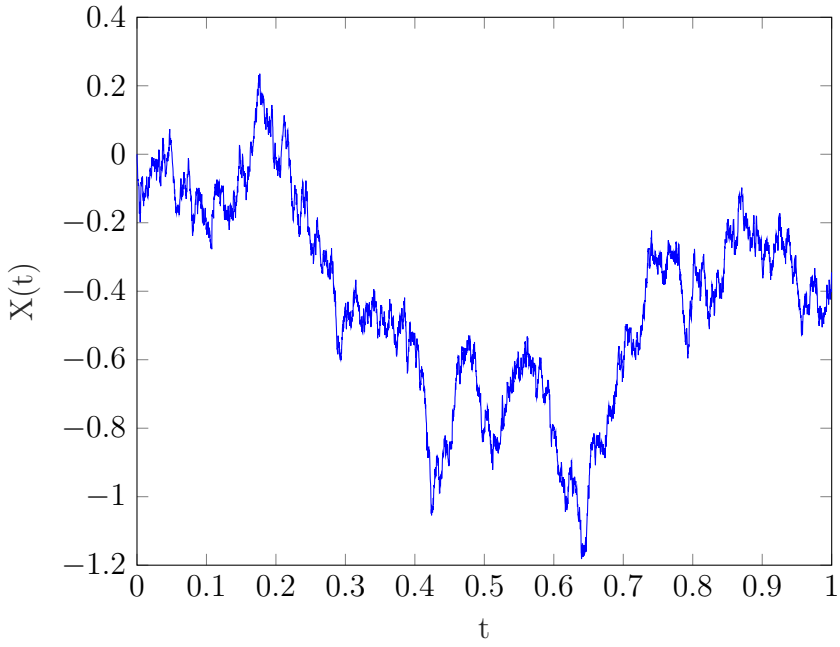

Figure 2.1: A simulated path of a Brownian motion on the domain $T = [0, 1]$

for $n \geq 1$, $(\lambda_1, \ldots, \lambda_n) \in \mathbb{R}^n$, $(t_1, \ldots, t_n) \in T^n$,

$$\mathbb{E}\left[\exp\left(i\sum_{j=1}^{n}\lambda_j X(t_j)\right)\right] = \exp\left(i\sum_{j=1}^{n}\lambda_j m(t_j)\right) \times \exp\left(-\frac{1}{2}\sum_{i,j=1}^{n}\lambda_i\lambda_j R(t_i, t_j)\right),$$

the field has a unique real valued Gaussian distribution, with mean value function m *and covariance function is* R.

Definition 2.1.12. A vector space G of centered Gaussian random variables, which is a closed subspace of $L^2(\Omega, \mathcal{A}, P)$ is called a *Gaussian space*. The Hilbert space $L^2(\Omega, \mathcal{A}, P)$ is equipped with the inner product and the corresponding induced norm

$$\langle X, Y\rangle_{L^2} = \mathbb{E}\left[XY\right],$$
$$\|X\|_{L^2} = \sqrt{\langle X, X\rangle_{L^2}}.$$

Example of a Gaussian space is

$$G = \left\{\sum_{i=1}^{d}\lambda_i X_i,\ (\lambda_1, \ldots, \lambda_d) \in \mathbb{R}^d\right\},$$

where $(X_1, \ldots, X_d)$ is a Gaussian random vector.

Definition 2.1.13. Let $(X(t),\ t \in T)$ be a centered Gaussian field. The subspace of $L^2(\Omega, \mathcal{A}, P)$ of the linear span of $(X(t),\ t \in T)$ and of their limits in L^2 is denoted

by

$$\mathcal{L}_X = \overline{\left\{ Z \text{ s.t. } \exists n \in \mathbb{N},\ \exists \lambda_i \in \mathbb{R},\ i = 1, \ldots, n \text{ with } Z = \sum_{i=1}^{n} \lambda_i X(t_i) \right\}}^{L^2}.$$

Next, the space

$$K_X = \{h_Z : T \to \mathbb{R} \text{ s.t. } \exists Z \in \mathcal{L}_X \text{ and } h_Z(t) = \mathbb{E}[ZX(t)]\}$$

equipped with the symmetric form $\langle h_{Z_1}, h_{Z_2} \rangle_{K_X} := \mathbb{E}[Z_1 Z_2]$ is called the *Reproducing Kernel Hilbert Space (RKHS)* of the Gaussian field X.

Proposition 2.1.3. *The map $h : \mathcal{L}_X \to K_X$ defined by $Z \mapsto h_Z$ is an injective linear map s.t. $\|h_Z\|_{K_X} = \|Z\|_{\mathcal{L}_X}$.*

From this it directly follows that for a Gaussian field X we have with the definitions above that

$$h_{X(t)}(s) = \mathbb{E}[X(t)X(s)] = R(t, s)$$

which tells us that finite linear combinations of the covariance function are dense in K_X. This can be seen by the fact that every $h_Z \in K_X$ corresponds to a $Z \in \mathcal{L}_X$, for which there is some $n \in \mathbb{N}$, $(\lambda_1, \ldots, \lambda_n) \in \mathbb{R}^n$ and $(t_1, \ldots, t_n) \in T^n$ s.t. $X^n \in \mathcal{L}_X$ has the L^2 limit Z,

$$\|h_{X^n} - h_Z\|_{K_X} = \|X^n - Z\|_{\mathcal{L}_X} \to 0 \text{ as } n \to \infty.$$

Next we also have two more properties which give reason to the name of reproducing. For a $h_Z \in K_X$ we have

$$\begin{aligned} \langle h_Z, R(t, \cdot) \rangle_{K_X} &= \mathbb{E}[ZX(t)] = h_Z(t), \\ \langle R(t, \cdot), R(s, \cdot) \rangle_{K_X} &= R(t, s). \end{aligned}$$

With this in mind and the fact that the covariance function of the Gaussian random field $(X(t),\ t \in T)$ is continuous, it can be shown that K_X is a separable Hilbert space if we also assume that X is separable. This definition is covered in [1], where the surrounding details are covered including how h, from Proposition 2.1.3, is an isomorphism. Now with K_X separable we can take an orthonormal basis of K_X which leads us to Theorem 2.1.5.

Theorem 2.1.5. *Let X be a centered Gaussian field and $(e_n)_{n \in \mathbb{N}}$ an orthonormal basis of K_X and recall h from Proposition 2.1.3. Next, denote by $\eta_n = h^{-1}(e_n)$ a random variable in $\mathcal{L}_X$. Then the variables $(\eta_n)_{n \in \mathbb{N}}$ are i.i.d. Gaussian random variables and constitute an orthonormal basis of $\mathcal{L}_X$. Also for $t \in T$, we have*

$$X(t) = \sum_{n=0}^{\infty} \eta_n e_n(t)$$

with convergence in $L^2(\Omega)$ and

$$R(t, \cdot) = \sum_{n=0}^{\infty} e_n(\cdot) e_n(t)$$

with convergence in K_X.

Definition 2.1.14. Two probability measures $\mathbb{P}$ and $\mathbb{Q}$ defined on the same probability space $(\Omega, \mathcal{A})$ are equivalent if and only if for all $A \in \mathcal{A}$ it holds that $\mathbb{P}(A) = 0$ if and only if $\mathbb{Q}(A) = 0$. On the other hand $\mathbb{P}$ and $\mathbb{Q}$ are orthogonal if there exists $A \in \mathcal{A}$ such that $\mathbb{P}(A) = 0$ and $Q(A) = 1$.

Given this definition we can state the following theorem.

Theorem 2.1.6. *The distributions of two Gaussian processes are either equivalent or orthogonal.*

The distribution of a Gaussian process is a Gaussian measure, a term which will be avoided to not confuse with what later will be defined as a Gaussian random measure.

Lemma 2.1.1. *The vector space defined as*

$$\left\{ h : T \to \mathbb{R} \text{ s.t., } \exists (a_n) \text{ with } h(t) = \sum_{n \geq 0} a_n \lambda_n \varphi_n(t), \ \sum_{n \geq 0} a_n^2 < \infty, \ \lambda_n \in \mathbb{R}^+ \right\}$$

equipped with the inner product $(h, g)_{K_X} = \sum_{n \geq 0} a_n b_n$ *where* $g = \sum_{n \geq 0} b_n \lambda_n \varphi_n(t)$, *and* $(\lambda_n \varphi_n)_{n \in \mathbb{N}}$ *is an orthonormal basis of* K_X, *is exactly the RKHS of* X, K_X.

2.1.3 Gaussian random measures

Gaussian random measures are important when we later will define a multifractional Brownian field (mBf), hence we start with a formal definition.

Definition 2.1.15. A *Gaussian random measure* on a measure space $(M, \mathcal{M}, \mu)$ is an isometry $\mathcal{I}$ from the Hilbert space $L^2(M, \mathcal{M}, \mu)$ onto a Gaussian space included in some $L^2(\Omega, \mathcal{A}, \mathbb{P})$.

Definition 2.1.16. A random measure $\mathcal{I}$ on a measure space $(M, \mathcal{M}, \mu)$ is called *independently scattered* if and only if for a sequence of measurable sets $(A_n)_{n \in \mathbb{N}} \subset \mathcal{M}$ s.t. $\mu(\cup_{n \in \mathbb{N}} A_n) < \infty$ then the random variables $\mathcal{I}(A_n)$ are independent if $(A_n)_{n \in \mathbb{N}}$ are mutually disjoint.

It can be shown that any Gaussian random measure satisfies this property.

Definition 2.1.17. Following Definition 2.1.15 and set $M = \mathbb{R}^d$, $\mathcal{M} = \mathcal{B}(\mathbb{R}^d)$ and $\mu(\mathrm{d}s) = \frac{\mathrm{d}s}{(2\pi)^{d/2}}$, then $\mathcal{I}$ is called a real valued *Brownian random measure* and will be denoted $W(\mathrm{d}s)$ onwards.

Proposition 2.1.4. *The following is true for a Brownian random measure* W. *For any* $f, g \in L^2(\mathbb{R}^d)$ *the random variable* $\int_{\mathbb{R}^d} f(s) W(\mathrm{d}s)$ *is a centered Gaussian variable with variance and covariance*

$$\mathbb{E}\left[\left(\int_{\mathbb{R}^d} f(s) W(\mathrm{d}s) \right)^2 \right] = \int_{\mathbb{R}^d} f(s)^2 \frac{\mathrm{d}s}{(2\pi)^{d/2}},$$
$$\mathbb{E}\left[\int_{\mathbb{R}^d} f(s) W(\mathrm{d}s) \int_{\mathbb{R}^d} g(s) W(\mathrm{d}s) \right] = \int_{\mathbb{R}^d} f(s) g(s) \frac{\mathrm{d}s}{(2\pi)^{d/2}}.$$

In other words, the last equality says that if f and g are orthogonal w.r.t. to the inner product of $L^2(\mathbb{R}^d)$ then the random variables $\int_{\mathbb{R}^d} f(s)W(\mathrm{d}s)$ and $\int_{\mathbb{R}^d} g(s)W(\mathrm{d}s)$ are independent.

Note that for a convergent series $\sum_{n\in\mathbb{N}} f_n$ in $L^2(\mathbb{R}^d)$ we have by Fubini–Tonelli

$$\int_{\mathbb{R}^d} \sum_{n\in\mathbb{N}} f_n(s)W(\mathrm{d}s) = \sum_{n\in\mathbb{N}} \int_{\mathbb{R}^d} f_n(s)W(\mathrm{d}s).$$

Implicitly we can construct a Brownian random measure by considering an orthonormal basis $(e_n)_{n\in\mathbb{N}}$ of $L^2(\mathbb{R}^d)$ and a sequence $(\eta_n)_{n\in\mathbb{N}}$ of i.i.d. $\mathcal{N}(0,1)$ r.v., then let

$$W(\mathrm{d}s) = \sum_{n\in\mathbb{N}} \eta_n e_n(s) \frac{\mathrm{d}s}{(2\pi)^{d/2}}. \tag{2.1}$$

This implies that

$$\int_{\mathbb{R}^d} f(s)W(\mathrm{d}s) = \sum_{n\in\mathbb{N}} \langle f, e_n\rangle_{L^2(\mathbb{R}^d)}\, \eta_n$$

holds for all $f \in L^2(\mathbb{R}^d)$, where

$$\langle f, e_n\rangle_{L^2(\mathbb{R}^d)} = \int_{\mathbb{R}^d} f(s)e_n(s)\frac{\mathrm{d}s}{(2\pi)^{d/2}}.$$

Definition 2.1.18. Let $W(\mathrm{d}s)$ be a real valued Brownian random measure, $\mathcal{F}$ be the space of complex valued functions $f \in L^2(\mathbb{R}^d, \mathbb{C})$ with $f(-\xi) = \overline{f(\xi)}$. Then for every $f \in \mathcal{F}$ we define the Fourier transform of $W(\mathrm{d}s)$, denoted $\widehat{W}(\mathrm{d}\xi)$, by

$$\int_{\mathbb{R}^d} f(\xi)\widehat{W}(\mathrm{d}\xi) := \int_{\mathbb{R}^d} \widehat{f}(s)W(\mathrm{d}s).$$

Now for a Brownian random measure of the form (2.1) the above definition yields a way to find the corresponding Fourier transform $\widehat{W}(\mathrm{d}\xi)$ explicitly

$$\begin{aligned}
\int_{\mathbb{R}^d} f(\xi)\widehat{W}(\mathrm{d}\xi) &= \int_{\mathbb{R}^d} \widehat{f}(s)W(\mathrm{d}s) \\
&= \sum_{n\in\mathbb{N}} \left\langle \widehat{f}, e_n \right\rangle_{L^2(\mathbb{R}^d)} \eta_n \\
&= \sum_{n\in\mathbb{N}} \langle f, \widehat{e}_n\rangle_{L^2(\mathbb{R}^d)}\, \eta_n \\
&= \sum_{n\in\mathbb{N}} \int_{\mathbb{R}^d} f(\xi)\overline{\widehat{e}_n(\xi)}\frac{\mathrm{d}\xi}{(2\pi)^{d/2}}\eta_n
\end{aligned}$$

where we use that

$$\begin{aligned}
\left\langle \widehat{f}, e_n \right\rangle_{L^2(\mathbb{R}^d)} &= \int_{\mathbb{R}^d} \widehat{f}(s)e_n(s)\,\mathrm{d}s \\
&= \int_{\mathbb{R}^d} f(\xi)\widehat{e_n}(\xi)\,\mathrm{d}\xi \\
&= \langle f, \widehat{e}_n\rangle_{L^2(\mathbb{R}^d)}\,.
\end{aligned}$$

Now with Fubini–Tonelli we have

$$\widehat{W}(\mathrm{d}\xi) = \sum_{n\in\mathbb{N}} \eta_n \overline{\widehat{e}_n(\xi)} \frac{\mathrm{d}\xi}{(2\pi)^{d/2}}. \tag{2.2}$$

Another important property which follows from Definition 2.1.18 and Proposition 2.1.4 is that for $f, g \in \mathcal{F}$

$$\begin{aligned} \mathbb{E}\left[\int_{\mathbb{R}^d} f(\xi)\widehat{W}(\mathrm{d}\xi) \int_{\mathbb{R}^d} g(\xi)\widehat{W}(\mathrm{d}\xi)\right] &= \mathbb{E}\left[\int_{\mathbb{R}^d} \widehat{f}(\xi) W(\mathrm{d}\xi) \int_{\mathbb{R}^d} \widehat{g}(\xi) W(\mathrm{d}\xi)\right] \\ &= \int_{\mathbb{R}^d} \widehat{f}(s)\widehat{g}(s) \frac{\mathrm{d}s}{(2\pi)^{d/2}} \end{aligned} \tag{2.3}$$

2.1.4 Stationary fields

Definition 2.1.19. A field $X = (X(t),\ t \in T)$ s.t. $\mathbb{E}\left[|X(t)|^2\right] < \infty$, $t \in T$ is called *weakly stationary* if the mean value is constant and if there exists a function r s.t. the covariance $R(t,s) = r(t-s)$. This function r is called the *autocovariance function* of X. The field X is called *strictly* (or *strongly*) *stationary* if it holds that for all $h \in T$ the distribution of $(X(t),\ t \in T)$ and $(X(t+s),\ t \in T)$ is equal, this is denoted in the following way

$$(X(t+s))_{t\in T} \overset{(\mathrm{d})}{=} (X(t))_{t\in T}.$$

It can be shown that a strictly stationary field with finite first and second moment is weakly stationary. Another property for Gaussian fields is that the field is strictly stationary if and only if it is weakly stationary.

Definition 2.1.20. For a weakly stationary field $(X(t),\ t \in T)$ the autocovariance function $r(t-s) = R(t,s)$ is a non-negative definite function in the sense of Definition 2.1.6. If r is continuous then by Bochner's theorem 2.1.2 there exists a symmetric measure μ on $\mathbb{R}^d$ s.t.

$$r(t) = \int_{\mathbb{R}^d} e^{it\xi} \mu(\mathrm{d}\xi).$$

This measure is called the *spectral measure* of the field X. If μ admits a density with respect to the Lebesgue measure $\mathrm{d}\xi$ then this density is called the *spectral density* of X.

Remark. Consider a centered stationary Gaussian field $(X(t),\ t \in T)$ with covariance $r(h) = \mathbb{E}\left[X(t+h)X(t)\right]$. Assume that r is a continuous function with the corresponding spectral measure $\mu(\mathrm{d}\xi) = f(\xi)\,\mathrm{d}\xi$. Observe that $r(h) = r(-h)$ and by Definition 2.1.20 we have that

$$r(h) = \int_{\mathbb{R}^d} e^{ih\xi} f(\xi)\,\mathrm{d}\xi.$$

This must then imply $f(\xi) = f(-\xi)$ and that f is a non-negative definite function. Next construct

$$Y(t) = (2\pi)^{d/4} \int_{\mathbb{R}^d} \sqrt{f(\xi)} e^{it\xi} \widehat{W}(\mathrm{d}\xi), \tag{2.4}$$

with W a real Brownian random measure. From Proposition 2.1.4 Y is a centered Gaussian field and its covariance function can be calculated with the isometry property defined above (2.3) and Parseval's formula [7],

$$\mathbb{E}\left[Y(t)Y(s)\right] = \int_{\mathbb{R}^d} f(\xi)e^{i(t-s)\xi}\,\mathrm{d}\xi = r(t-s).$$

This shows that X and Y have the same mean and covariance, now since they are Gaussian this shows that they have the same distribution. The representation of Y is called the *spectral representation* of X.

Recall Example 2.1.1 of the Brownian motion. This process is not stationary since for example the variance is not the same over time. However often one might discuss stationarity of a field and not explicitly mean the field itself but its increments, such a field is called a field with stationary increments.

Definition 2.1.21. A field $(X(t),\ t \in T)$ s.t.

$$(X(t+h) - X(s+h))_{t\in T} \overset{(\mathrm{d})}{=} (X(t) - X(s))_{t\in T}$$

for all $s, h \in T = \mathbb{R}^d$ is called a field with *stationary increments*.

Previously the spectral representation of the covariance of a stationary field was shown and now the corresponding representation for fields with stationary increments will be defined. Let $(X(t),\ t \in T)$ be a centered field with stationary increments with finite variance, $X(0) = 0$ a.s. and continuous covariance. Following the steps in [4] with this setting it can be shown that the spectral representation for a Gaussian field with stationary increments, given a spectral density f, is the following

$$X(t) \overset{(\mathrm{d})}{=} (2\pi)^{d/4} \int_{\mathbb{R}^d} (e^{it\xi} - 1)\sqrt{f(\xi)}\widehat{W}(\mathrm{d}\xi) + t^\top N,$$

where N is a centered Gaussian random vector with covariance Σ, which is independent of the integral representation for all $t \in \mathbb{R}^d$. Both t and N are column vectors and the dot product of the vectors in $\mathbb{R}^d$ is defined as $t^\top N = \sum_{i=1}^d t_i N_i$.

2.1.5 Regularity

Another important part of this background chapter is to understand the regularity of the fields.

Definition 2.1.22. Let $f : \mathbb{R}^d \to \mathbb{R}$ be a function s.t. there exists a constant $C > 0$ and $0 < H < 1$ such that

$$|f(t) - f(s)| \leq C \left\|t - s\right\|^H,$$

for $t, s \in \mathbb{R}^d$. A function that fulfills this property is called *H-Hölder continuous*. The set of such functions on $[0,1]^d$ is denoted by $\mathcal{C}^H$.

Definition 2.1.23. Let $f : \mathbb{R}^d \to \mathbb{R}$ be a function s.t. on every compact set $K \subset \mathbb{R}^d$ there exists a $C(K) > 0$ and $0 < H < 1$ such that

$$|f(t) - f(s)| \leq C(K) \left\|t - s\right\|^H,$$

for $t, s \in K$. Then f is called *locally H-Hölder continuous*.

Both these definitions yield the inclusion that if $H' < H$, then H-Hölder continuous functions are also H'-Hölder continuous. This Hölder exponent will be referred to as both Hölder exponent as well as the Hurst parameter.

Definition 2.1.24. A real valued function f defined in a neighbourhood of t has a *pointwise Hölder exponent* H if

$$H(t) = \sup\left\{H' : \lim_{\|h\|\to 0} \frac{f(t+h) - f(t)}{\|h\|^{H'}} = 0\right\} \tag{2.5}$$

Theorem 2.1.7 (Kolmogorov–Chentsov's theorem)**.** *Let* $(X(t),\ t \in [A,B]^d)$ *be a random field on a probability space* $(\Omega, \mathcal{A}, \mathbb{P})$*. If there exist three positive constants* $\alpha,\ \beta,\ C$ *s.t., for* $t, s \in [A,B]^d$

$$\mathbb{E}\left[|X(t) - X(s)|^\alpha\right] \leq C\,\|t-s\|^{d+\beta},$$

then there exists a locally $\gamma-$*Hölder continuous modification* $\widetilde{X}$ *of* X *for every* $\gamma < \beta/\alpha$*. That is, there exist a random variable* h *and a constant* $\delta > 0$ *s.t.*

$$\mathbb{P}\left(\omega : \sup_{\|t-s\|\leq h(\omega)} \frac{|\widetilde{X}(t)(\omega) - \widetilde{X}(s)(\omega)|}{\|t-s\|^\gamma} \leq \delta\right) = 1.$$

With this theorem we can show that the Brownian motion from Example 2.1.1 is locally $\gamma-$Hölder continuous for all $\gamma < \frac{1}{2} - \varepsilon,\ \varepsilon > 0$. This theorem is proved in [11].

Theorem 2.1.8. *Let* $(X(t),\ t \in [A,B])$ *be a stochastic process s.t. there exist positive constants* $\alpha_0,\ \beta_0,\ C_0$ *s.t. for* $t, h \in [A,B]$ *such that* $t + h \in [A,B]$

$$\mathbb{E}\left[|X(t+h) - X(t)|^{\alpha_0}\right] \leq C_0|h|^{1+\beta_0}.$$

Assume there exist three other positive constants $\alpha_1,\ \beta_1 > \alpha_1,\ C_1$ *s.t. for all* $t, h \in [A,B]$ *such that* $t-h,\ t+h \in [A,B]$ *it holds that*

$$\mathbb{E}\left[|X(t+h) + X(t-h) - 2X(t)|^{\alpha_1}\right] \leq C_1|h|^{1+\beta_1}.$$

Then there exists a modification of X *which has almost surely continuous differentiable sample paths.*

The next part will cover convergence and hence we recall Definition 2.1.2 of the finite dimensional distribution of a field.

Definition 2.1.25. Let $(X^n,\ n \in \mathbb{N})$ be a sequence of random fields, then we say that $(X^n,\ n \in \mathbb{N})$ *converges in distribution* to the random field X for all finite dimensional margins of the field, if, $k \in \mathbb{N}$ and $(t_1, \ldots, t_k) \in T^k$ it holds that

$$\lim_{n\to\infty}(X^n(t_1), \ldots, X^n(t_k)) \overset{(\mathrm{d})}{=} (X(t_1), \ldots, X(t_k)).$$

Remark. Consider the space of continuous functions $C^0([A,B]^d)$ onto $\mathbb{R}$ with the topology induced by the uniform metric distance, that is

$$\rho(f,g) = \sup_{t\in[A,B]^d} |f(t) - g(t)|.$$

This topology corresponds to the uniform convergence, which is central in our next definition.

Definition 2.1.26. Let $(X^n,\ n \in \mathbb{N})$ be a sequence of continuous random fields. We say that $(X^n,\ n \in \mathbb{N})$ converges in distribution to the continuous random field X on the space of continuous functions endowed with the topology of the uniform convergence, if, for every bounded continuous functional $F : C^0 \to \mathbb{R}$

$$\lim_{n\to\infty} \mathbb{E}\left[F(X^n)\right] = \mathbb{E}\left[F(X)\right].$$

Proposition 2.1.5. *Convergence in distribution on the space of continuous functions endowed with the topology of the uniform convergence implies the convergence of finite dimensional margins.*

Theorem 2.1.9. *Let $(X^n,\ n \in \mathbb{N})$ and X be C^0-valued random fields s.t. for all $k \in \mathbb{N}$ and $t_1,\dots,t_k \in [A,B]^d$ the finite dimensional distributions of $(X^n(t_1),\dots,X^n(t_k))$ converge to $(X(t_1),\dots,X(t_k))$. If there exist three positive constants $\alpha,\ \beta,\ C$ s.t. for $t,s \in [A,B]^d$*

$$\sup_{n\in\mathbb{N}} \mathbb{E}\left[|X^n(t) - X^n(s)|^\alpha\right] \le C\left\|t-s\right\|^{d+\beta},$$

then $(X^n,\ n \in \mathbb{N})$ converges to the continuous field X in distribution on the space of continuous functions with respect to the topology of the uniform convergence.

2.2 Fractal analysis

2.2.1 Fractional operators

To define fractional fields in the sense of an integral representation we must consider fractional operators. To this end we refer the details of the derivations in [4] which is based on Fourier analysis. This approach leads to the d-dimensional harmonizable fractional operator $\widetilde{\mathcal{I}}_H : L^2(\mathbb{R}^d) \to L^2(\mathbb{R}^d)$ defined as

$$\widetilde{\mathcal{I}}_H(f(t)) = \int_{\mathbb{R}^d} \overline{\widehat{f(\xi)}} \frac{(e^{-it\xi}-1)}{\left\|\xi\right\|^{H+d/2}} \frac{\mathrm{d}\xi}{(2\pi)^{d/2}}. \tag{2.6}$$

Clearly the operator $\widetilde{\mathcal{I}}_H$ is defined on $L^2(\mathbb{R}^d)$ since $k(\xi) = \frac{(e^{-it\xi}-1)}{\left\|\xi\right\|^{H+d/2}} \in L^2(\mathbb{R}^d)$. This is directly related to Gaussian random measures and later the integral representation of fractional Brownian motion. One can also with the use of Plancherel's theorem [7] rewrite the expression from the spectral frequency form to the so-called moving-average fractional operator:

$$\widetilde{\mathcal{I}}_H(f(t)) = C\int_{\mathbb{R}^d} f(s)(\left\|t-s\right\|^{H-d/2} - \left\|s\right\|^{H-d/2}) \frac{\mathrm{d}s}{(2\pi)^{d/2}}. \tag{2.7}$$

Now following the steps in [6] we will define the Hausdorff measure.

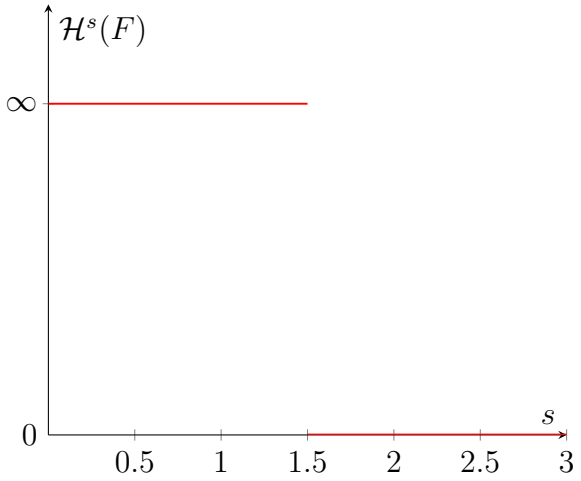

Figure 2.2: The Hausdorff measure $\mathcal{H}^s$ of the graph of Brownian motion

Definition 2.2.1. Let $\{U_i\}$ be a countable or finite collection of sets of diameter at most δ that covers a set F, then $\{U_i\}$ is a said to be a *δ-cover* of F. Now suppose F is a subset of $\mathbb{R}^d$ and s is a non-negative number, then define for any $\delta > 0$ the measure

$$\mathcal{H}^s_\delta(F) = \inf\left\{\sum_{i=1}^{\infty} \operatorname{diam}(U_i)^s : \ \operatorname{diam}(U_i) < \delta, \ F \subset \bigcup_i^{\infty}\{U_i\}\right\}.$$

Then by letting $\delta \to 0$ the *s-dimensional Hausdorff measure* of F is obtained,

$$\mathcal{H}^s(F) = \lim_{\delta \to 0} \mathcal{H}^s_\delta(F).$$

Now an important property of the Hausdorff measure is the fact that it yields either infinity or 0 except for possibly one value of s for each set F. This value s is the *Hausdorff dimension* and is defined as

$$\dim_{\mathcal{H}}(F) = \inf\{s : \ \mathcal{H}^s(F) = 0\} = \sup\{s : \ \mathcal{H}^s(F) = \infty\}. \tag{2.8}$$

Example 2.2.1. Continuing on Example 2.1.1 with the Brownian motion it can be shown that this process has the Hausdorff dimension $\dim_{\mathcal{H}}(B) < \frac{3}{2}$. In Figure 2.2 the Hausdorff measure of the graph of B is illustrated to express how the measure works and not in a formal sense. In Lemma 2.2.1 the Hausdorff dimension is directly related to the Hurst parameter.

This following property relates the Hausdorff dimension to the Hurst parameter H which will become more essential when we are defining fractional Brownian fields.

Lemma 2.2.1. *For $0 < H < 1$ we let f be a H-Hölder continuous function. Then $\dim_{\mathcal{H}}\{(t, f(t)) : \ t \in [0,1]\} \leq 2 - H$.*

Lemma 2.2.2. *Let F be a Borel set in $\mathbb{R}^d$. Define the s-energy of F associated with a given probability measure μ*

$$I_s(\mu) = \int_{F^2} \frac{\mu(\mathrm{d}x)\mu(\mathrm{d}y)}{|x-y|^s}.$$

If there exists a probability measure μ on F with

$$I_s(\mu) < \infty$$

then $\dim_{\mathcal{H}}(F) \geq s$. *If* $\mathcal{H}^s(F) > 0$ *then there exists a probability measure* μ *on* F *with* $I_t(\mu) < \infty$ *for all* $t < s$.

2.2.2 Lemarié–Meyer basis

We finish this section by doing a brief introduction of the Lemarié–Meyer basis that will be used as an orthonormal basis for $L^2(\mathbb{R})$. There exists a function $\psi^{(1)} \in L^2(\mathbb{R})$ such that the support of its Fourier transform is included in $\{\frac{2\pi}{3} < |\xi| < \frac{8\pi}{3}\}$ and such that the functions

$$\psi^{(1)}_{j,k}(x) = 2^{j/2}\psi^{(1)}(2^j x - k), \tag{2.9}$$

where $j, k \in \mathbb{Z}$, constitute an orthonormal basis of $L^2(\mathbb{R})$. This index and index set is denoted by $\lambda = (j, k, l) \in \Lambda = \mathbb{Z} \times \mathbb{Z} \times \{1\}$. You can also show that there is another basis of $L^2(\mathbb{R})$ consisting of the orthonormal functions $(\psi^{(l)}_{j,k})_{\lambda \in \Lambda^+}$ where $\Lambda^+ = \mathbb{N} \times \mathbb{Z} \times \{1\} \cup \{0\} \times \mathbb{Z} \times \{0\}$, and $\psi^{(0)}_{0,k} = \psi^{(0)}(x-k)$ for a function $\psi^{(0)} \in L^2(\mathbb{R})$.

The important part of this basis is a localization property. The inverse Fourier transform yields

$$\psi^{(1)}(x) = \int_{\frac{2\pi}{3} < |\xi| < \frac{8\pi}{3}} e^{-ix\xi} \widehat{\psi^{(1)}}(\xi) \frac{\mathrm{d}\xi}{(2\pi)^{1/2}},$$

which implies that $\psi^{(1)} \in C^\infty$. One can also show that

$$|\psi^{(1)}(x)| \leq \frac{C(K)}{1 + |x|^K} \quad \text{and}$$

$$|\psi_\lambda(x)| \leq \frac{C(K)2^{j/2}}{1 + |2^j x - k|^K}$$

for all $K \in \mathbb{N}$ where $\psi_\lambda(x) = \psi^{(1)}_{j,k}(x)$.

2.3 Fractional Brownian fields

In this part of the background chapter we will finally be able to define fractional Brownian motion and in the case of dimension $d > 1$ fractional Brownian fields. The section will begin by explaining an important property of fractional Brownian fields, which is self-similarity. Then we will go on to the theorems that give rise to the definition of the fractional Brownian motion.

2.3.1 Self-similarity

First, let us consider the deterministic case. The most trivial case is a straight line, each part of the line is similar to the whole, simply by a linear scaling. Self-similarity arises in both trivial and non-trivial cases. For example some of the more famous fractals are self-similar. The name fractals come from the fact that the set does not have an integer Hausdorff dimension, but a fractional Hausdorff dimension.

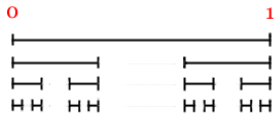

Figure 2.3: The Cantor set

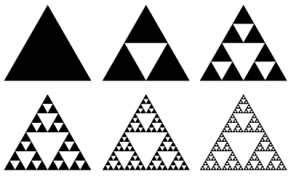

Figure 2.4: The Sierpinski triangle in $\mathbb{R}^2$

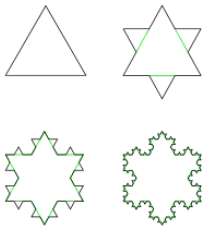

Figure 2.5: The von Koch snowflake

Example 2.3.1. In Figures 2.3-2.5 we present some iterations of three different fractals that are self-similar and commonly referred to. First we have the Cantor set which has the Hausdorff dimension $\log_3(2) \approx 0.6309$, second the Sierpinski triangle with Hausdorff dimension $\log_2(3) \approx 1.5850$ and third we have the Koch snowflake which consists of three Koch curves of Hausdorff dimension $\log_3(4) \approx 1.2619$.

Formally we say that a function f is *self-similar* if it is similar to each part of itself. That is $f(\varepsilon x) = \varepsilon^\alpha f(x)$ for every $\varepsilon > 0$, $x \in \mathbb{R}^d$ and some $\alpha > 0$, which is called the *order of the homogeneous function* f. In the multidimensional case one usually assumes rotational invariance and hence the only self-similar function is

$$f(x) = C \|x\|^\alpha .$$

Next we want to find the corresponding case for stochastic self-similarity. This is usually done in a spectral analysis sense. Another result which is useful to use here is that the Fourier transform of a homogeneous function of order α is a homogeneous function of order $-(d+\alpha)$. Hence one has for a function f that is of order α

$$\int_{\mathbb{R}^d} e^{ix\varepsilon\xi} f(x) \frac{\mathrm{d}x}{(2\pi)^{d/2}} = \varepsilon^{-d-\alpha} \widehat{f}(\xi).$$

If we again consider the function f defined previously, we have

$$\int_{\mathbb{R}^d} \frac{e^{ix\xi} - 1}{\|\xi\|^{d+\alpha}} \frac{\mathrm{d}\xi}{(2\pi)^{d/2}} = C_\alpha \|x\|^\alpha .$$

Definition 2.3.1. A *H-self-similar* field satisfies

$$(X(\varepsilon t))_{t\in\mathbb{R}^d} \overset{(\mathrm{d})}{=} \varepsilon^H (X(t))_{t\in\mathbb{R}^d} \tag{2.10}$$

for every $\varepsilon > 0$.

2.3.2 Fractional Brownian motion

Before going to a more general dimension d we will devote some time to the one dimensional case. Now recalling Definition 2.1.21 of stationary increments we present an important proposition.

Proposition 2.3.1. *Let $(X(t),\ t \in \mathbb{R})$ be a non-constant real valued H-self-similar process with stationary increments. Assume that $\mathbb{E}[X(t)^2] < \infty$ for all $t \in \mathbb{R}$ and also $\lim_{\varepsilon \to 0} X(\varepsilon) \overset{(d)}{=} X(0)$. Then $0 \leq H \leq 1$ and $X(0) \overset{a.s.}{=} 0$. Moreover the covariance of the second order process X is determined up to a multiplicative constant by:*

$$\begin{aligned} R(s,t) &= \mathbb{E}[X(s)X(t)] \\ &= \frac{\mathbb{E}[X(1)^2]}{2}\left(|s|^{2H} + |t|^{2H} - |s-t|^{2H}\right). \end{aligned}$$

Also, if $0 < H < 1$ then $\mathbb{E}[X(t)] = 0$ for all t, and if $H = 1$ then $X(t) = tX(1)$.

Corollary 2.3.1. *Let $0 < H < 1$ and $V > 0$. Then there exists only one Gaussian process $(B_H(t))_{t \in \mathbb{R}}$ which is H-self-similar with stationary increments and such that $\mathrm{Var}(B_H(1)) = V$. This process is called fractional Brownian motion (denoted fBm) and it is a centered Gaussian process with covariance function R given by:*

$$R(s,t) = \frac{V}{2}\left(|s|^{2H} + |t|^{2H} - |s-t|^{2H}\right).$$

The spectral measure of R is $\frac{V\,\mathrm{d}\xi}{C_H|\xi|^{2H+1}(2\pi)^{1/2}}$, where $C_H = \frac{\sqrt{\pi}}{H\Gamma(2H)\sin(H\pi)\sqrt{2}}$. Also

$$\mathbb{E}\left[(B_H(t) - B_H(s))^2\right] = V|t-s|^{2H}.$$

A fractional Brownian motion is called a standard fractional Brownian motion if $V = 1$.

Example 2.3.2. We are now ready to show how trajectories of a fBm look like. This is illustrated in Figure 2.6 for Hurst parameters of 0.2 and 0.8. These are simulated with two different discretization levels which will be discussed in the next chapter where approximation of these processes will be investigated.

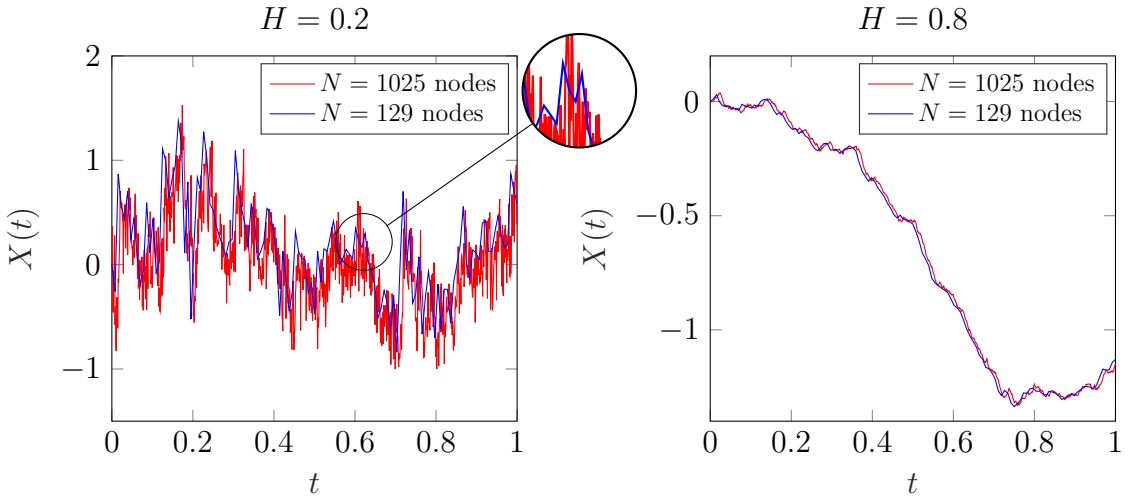

Figure 2.6: Sample paths of two fractional Brownian motions with Hurst parameter $H = 0.2$ to the left and $H = 0.8$ to the right, both are simulated with two discretizations

With this characterization of a fractional Brownian motion we can quickly deduce that by setting $H = \frac{1}{2}$ it becomes an ordinary Brownian motion which we defined in Definition 2.1.10.

Corollary 2.3.2. *If $(s_1, \dots, s_n) \in \mathbb{R}^n$ s.t. $s_i \neq s_j$ for $i \neq j$, then the matrix $(R(s_i, s_j))$ is a $n \times n$ symmetric matrix which is positive definite and $(B_H(s_1), \dots, B_H(s_n))$ are linearly independent almost surely. That is for $(a_1, \dots, a_n) \in \mathbb{R}^n$ s.t. $\sum_{i=1}^n a_i B_H(s_i) = 0$ implies that $a_1 = \cdots = a_n = 0$ almost surely.*

Proposition 2.3.2. *Define a one to one correspondence $\mathcal{I}_H$ from $L^2(\mathbb{R})$ onto the RKHS of fractional Brownian motion, denoted K_{B_H}, as*

$$\mathcal{I}_H(\psi)(y) = \int_{\mathbb{R}} \frac{e^{-iy\xi} - 1}{C_H^{1/2} |\xi|^{H+1/2}} \overline{\widehat{\psi}(\xi)} \frac{\mathrm{d}\xi}{(2\pi)^{1/2}}$$

for every $\psi \in L^2(\mathbb{R})$. The RKHS of fractional Brownian motion can then be written as

$$K_{B_H} = \{\phi : \ \exists \psi \in L^2(\mathbb{R}) \text{ s.t. } \phi = \mathcal{I}_H(\psi)\}.$$

Finally, $\mathcal{I}_H$ is an isometry s.t.

$$\langle \mathcal{I}_H(\psi_1), \mathcal{I}_H(\psi_2) \rangle_{K_{B_H}} = \langle \psi_1, \psi_2 \rangle_{L^2} .$$

Next we want to define the integral representation of fractional Brownian motion. Let $\Lambda = \mathbb{Z} \times \mathbb{Z} \times \{1\}$ and $\Lambda^+ = \mathbb{N} \times \mathbb{Z} \times \{1\} \cup \{0\} \times \mathbb{Z} \times \{0\}$.

Theorem 2.3.1. *Denote by $\varphi_\lambda = \mathcal{I}_H(\psi_\lambda)$ for $\lambda \in \Lambda^+$ an orthonormal basis for the RKHS K_{B_H} and let $(\eta_\lambda)_{\lambda \in \Lambda^+}$ be the corresponding sequence of i.i.d. standard*

Gaussian variables. One gets the following representation of fractional Brownian motion

$$B_H(t) = \sum_{\lambda\in\Lambda^+} \varphi_\lambda(t)\eta_\lambda.$$

This series representation converges in both $L^2(\Omega)$ and in almost sure sense for the uniform convergence on compact intervals. Next, if one considers the Brownian random measure defined in (2.2) associated to the Fourier transform of the Lemarié–Meyer basis, that is,

$$\widehat{W^+}(\mathrm{d}\xi) = \sum_{\lambda\in\Lambda^+} \overline{\widehat{\psi_\lambda}(\xi)}\eta_\lambda \,\mathrm{d}\xi,$$

then the harmonizable representation of fractional Brownian motion becomes

$$B_H(t) = \int_{\mathbb{R}} \frac{e^{-it\xi}-1}{C_H^{1/2}|\xi|^{H+1/2}} \widehat{W^+}(\mathrm{d}\xi).$$

There is a corresponding representation where one defines an orthonormal basis of $L^2(\mathbb{R})$ indexed by Λ instead. In the next theorem we introduce the moving average representation of the fractional Brownian motion.

Theorem 2.3.2. *Let $\widehat{W}(\mathrm{d}\xi) = \sum_{\lambda\in\Lambda} \overline{\widehat{\psi}_\lambda(\xi)}\eta_\lambda \,\mathrm{d}\xi$ be the Brownian random measure associated to the Fourier transform of the Lemarié–Meyer basis, then denote the Brownian random measure by $W(\mathrm{d}s) = \sum_{\lambda\in\Lambda} \psi_\lambda(s)\eta_\lambda \,\mathrm{d}s$. Now for $0 < H < 1$ it holds that*

$$\int_{\mathbb{R}} \frac{e^{-it\xi}-1}{C_H^{1/2}|\xi|^{1/2+H}} \widehat{W}(\mathrm{d}\xi) = \frac{D(H)}{C_H^{1/2}} \int_{\mathbb{R}} \left(|t-s|^{H-1/2} - |s|^{H-1/2}\right) W(\mathrm{d}s) \quad \text{a.s.},$$

where

$$D(H) = \frac{2^{-H}\Gamma(5/4-H/2)}{\Gamma(H/2+1/4)|1/4-H/2|}.$$

The interpretation of $|s|^0$ for $H = 1/2$ is $|s|^0 := \ln(1/|s|)$.

Theorem 2.3.3. *For every $H' < H$ there exists a modification of B_H s.t.*

$$\mathbb{P}\left(\sup_{\substack{|s-t|<\varepsilon(\omega)\\ |s|,|t|\le 1}} \left(\frac{B_H(t)-B_H(s)}{|t-s|^{H'}} \right) \le \delta \right) = 1$$

where ε is a positive random variable and $\delta > 0$. Also the pointwise Hölder exponent for every $t \in \mathbb{R}$:

$$\sup\left(H' : \lim_{\varepsilon\to 0} \frac{B_H(t+\varepsilon)-B_H(t)}{|\varepsilon|^{H'}} = 0 \right) = H.$$

Theorem 2.3.4. *The Hausdorff dimension defined in (2.8) of the graph of a fractional Brownian motion with Hurst exponent H,*

$$\{(s, B_H(s)) :\ 0 \le s \le 1\},$$

is $2-H$.

2.3.3 Fractional Brownian fields

Now we are ready to return to the general case of d dimensions.

Definition 2.3.2. The standard *fractional Brownian field* (fBf for short) is a centered Gaussian field and its covariance is given by

$$R(x,y) = \frac{1}{2}\left(\|x\|^{2H} + \|y\|^{2H} - \|x-y\|^{2H}\right).$$

Its harmonizable representation is given by

$$X(x) \overset{(\mathrm{d})}{=} \int_{\mathbb{R}^d} \frac{e^{-ix\xi} - 1}{C_H^{1/2}\,\|\xi\|^{H+d/2}} \widehat{W}(\mathrm{d}\xi),$$

where $\xi = (\xi_1, \ldots, \xi_d)$ and the constant C_H is defined by

$$\begin{aligned} C_H &= \int_{\mathbb{R}^d} \frac{2(1-\cos(\xi_1))}{\|\xi\|^{d+2H}} \frac{\mathrm{d}\xi}{(2\pi)^{d/2}} \\ &= \frac{\pi^{1/2}\Gamma(H+1/2)}{2^{d/2}H\Gamma(2H)\sin(\pi H)\Gamma(H+d/2)}, \end{aligned}$$

Finally the variance of the increments is given by

$$\mathbb{E}\left[(B_H(x) - B_H(y))^2\right] = \|x-y\|^{2H}.$$

With this setting we can also note that the isometry operator $\mathcal{I}_H : L^2(\mathbb{R}) \to K_{B_H}$, defined in Proposition 2.3.2 can be extended to higher dimensions simply by replacing the absolute value with the Euclidean norm raised to the power of $H + d/2$.

Example 2.3.3. We generalize Example 2.3.2 to the two-dimensional case on the domain of the unit square. This is illustrated in Figure 2.7 with Hurst parameter $H = 0.2$ where we see how the field can simulate the texture of a cloud by using an appropriate color map. In Figure 2.8 we have the corresponding case for a Hurst parameter of $H = 0.8$.

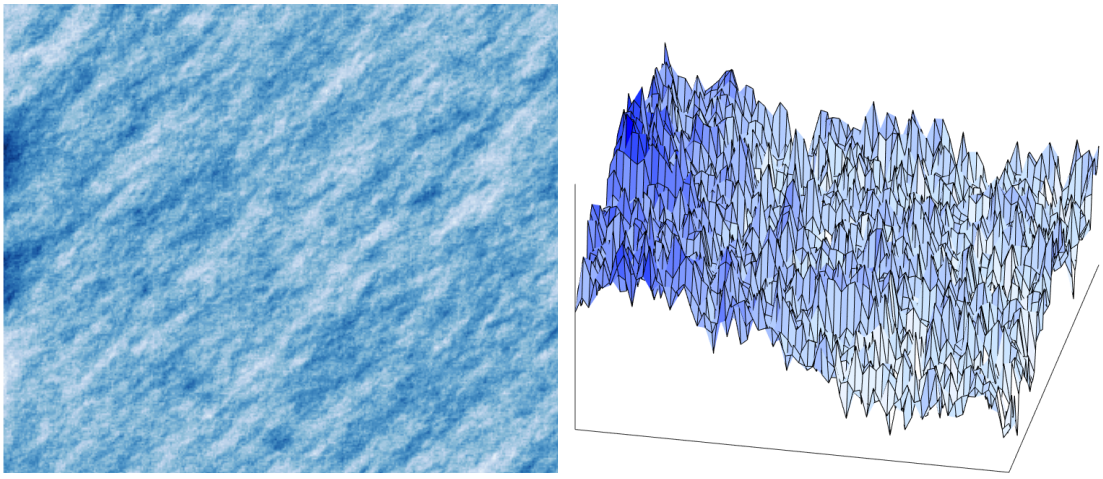

Figure 2.7: Two illustrations of the same generated fractional Brownian field with Hurst parameter $H = 0.2$. To the left the field is viewed from the z-axis in the direction onto the field while on the right we view it from the side

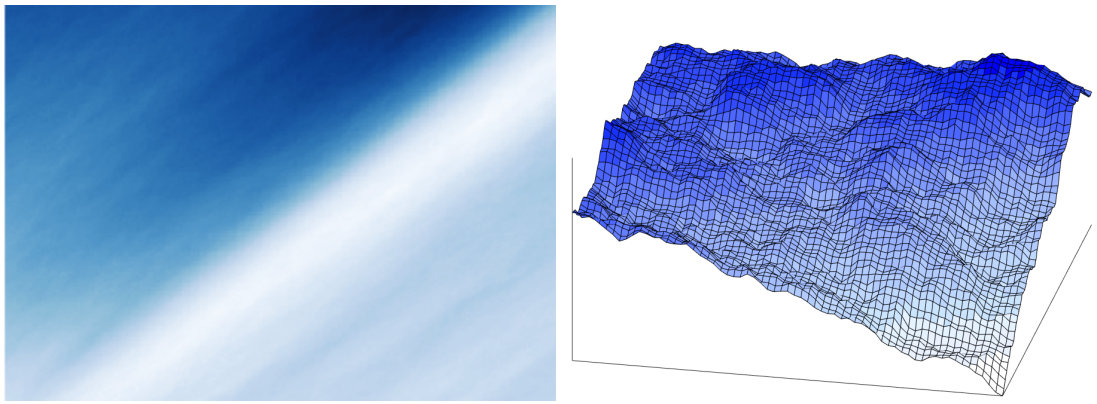

Figure 2.8: Two illustrations of the same generated fractional Brownian field with Hurst parameter $H = 0.8$. To the left the field is viewed from the z-axis in the direction onto the field while on the right we view it from the side

2.4 Multifractional Brownian fields

In this report we have so far introduced different concepts that relate to both stationarity and self-similarity. The aim is now to extend our understanding to cover another important property, namely the non-stationarity. By considering a varying *Hurst parameter* H, which controls the regularity of the field, we achieve a multifractional field which in turn is non-stationary in a global setting. Let $h : T \to (0, 1)$ be the function controlling the Hurst parameter.

2.4.1 Asymptotic self-similarity

Definition 2.4.1. A field $(Y(x))_{x\in\mathbb{R}^d}$ is *locally asymptotically self-similar* (lass for short) at point x if

$$\lim_{\varepsilon\to 0^+} \left(\frac{Y(x+\varepsilon u) - Y(x)}{\varepsilon^{h(x)}} \right)_{u\in\mathbb{R}^d} \overset{(\mathrm{d})}{=} (T_x(u))_{u\in\mathbb{R}^d},$$

where the non-degenerate field $(T_x(u))_{u\in\mathbb{R}^d}$ is called the tangent field at point x of Y and the limit is in distribution for all finite dimensional margins of the field. Furthermore, the field is lass with multifractional function h if for $x \in \mathbb{R}^d$, it is lass at point x with index $h(x)$.

Proposition 2.4.1. *A H-self-similar field Y with stationary increments is lass. More precisely for $x \in \mathbb{R}^d$*

$$\lim_{\varepsilon\to 0^+} \left(\frac{Y(x+\varepsilon u) - Y(x)}{\varepsilon^{H}} \right)_{u\in\mathbb{R}^d} \overset{(\mathrm{d})}{=} (Y(u))_{u\in\mathbb{R}^d}.$$

Definition 2.4.2. A field $(Y(x))_{x\in\mathbb{R}^d}$ is *strongly locally asymptotically self-similar* (slass for short) at point x if

$$\lim_{\varepsilon\to 0^+} \left(\frac{Y(x+\varepsilon u) - Y(x)}{\varepsilon^{h(x)}} \right)_{u\in\mathbb{R}^d} \overset{(\mathrm{d})}{=} (T_x(u))_{u\in\mathbb{R}^d},$$

where the non-degenerate field $(T_x(u))_{u\in\mathbb{R}^d}$ is called the tangent field at point x of Y and the limit is in distribution on the space of continuous functions endowed with the topology of the uniform convergence on every compact. Furthermore, the field is strongly lass with multifractional function h if for all $x \in \mathbb{R}^d$, it is strongly lass at the point x with index $h(x)$.

The only difference between the definitions of lass and slass is in the sense of convergence of the limit. Recall Proposition 2.1.5 which states the hierarchy of the two types of convergence, for these definitions slass implies lass.

Definition 2.4.3. A field $(Y(x))_{x\in\mathbb{R}^d}$ is *H-asymptotically self-similar* (∞-ass) at infinity if

$$\lim_{R\to\infty}\left(\frac{Y(Ru)}{R^H}\right)_{u\in\mathbb{R}^d} \overset{(\mathrm{d})}{=} (T(u))_{u\in\mathbb{R}^d},$$

where the non-degenerate field $(T(u))_{u\in\mathbb{R}^d}$ is called the tangent field at infinity of Y and the limit is in distribution for all finite dimensional margins of the field.

2.4.2 Fields

Definition 2.4.4. A field $(Y(x))_{x\in\mathbb{R}^d}$ is called a *filtered white noise* (fwn for short), if it admits the harmonizable representation

$$Y(x) \overset{(\mathrm{d})}{=} \int_{\mathbb{R}^d} (e^{-ix\xi} - 1)g(x,\xi)\ \widehat{\mathrm{d}\xi},$$

where for $x \in \mathbb{R}^d$ we have $(e^{-ix\xi} - 1)g(x,\xi) \in L^2(\mathbb{R}^d)$ and

$$g(x,\xi) = \frac{a(x)}{\|\xi\|^{H+d/2}} + r(x,\xi),$$

with $0 < H < 1$. It is also required that $a(x) \neq 0$ is a real valued C^2 function and that $r \in C^2$ with $\overline{r(x,\xi)} = r(x,-\xi)$. The final condition is that for $m, n \in \{0,1,2\}$, there exists a $C > 0$ and a $\eta > H$ s.t.

$$\left|\frac{\partial^{m+n}}{\partial x^m \partial \xi^n} r(x,\xi)\right| \leq \frac{C}{\|\xi\|^{\eta+n+d/2}},$$

for all $\xi, x \in \mathbb{R}^d$.

Proposition 2.4.2. *A filtered white noise $(Y(x))_{x\in\mathbb{R}^d}$ is strongly locally self-similar with a multifractional function constantly equal to H. More precisely, for $x \in \mathbb{R}^d$*

$$\lim_{\varepsilon\to 0^+}\left(\frac{Y(x+\varepsilon u) - Y(x)}{\varepsilon^H}\right)_{u\in\mathbb{R}^d} \overset{(\mathrm{d})}{=} C_H^{1/2} a(x)(B_H(u))_{u\in\mathbb{R}^d},$$

where the limit is in distribution on the space of continuous functions endowed with the topology of the uniform convergence on every compact.

Finally we reach the most desired definition, which our thesis relies on, namely that of the multifractional Brownian field.

Definition 2.4.5. Let $h : \mathbb{R}^d \mapsto (0,1)$ be a measurable function. A real valued field is called a *multifractional Brownian field* (mBf for short) with multifractional function h, if it admits the harmonizable representation

$$B_h(x) \overset{(\mathrm{d})}{=} \frac{1}{(C(h(x)))^{1/2}} \int_{\mathbb{R}^d} \frac{e^{-ix\xi} - 1}{\|\xi\|^{d/2+h(x)}} \widehat{W}(\mathrm{d}\xi),$$

where the normalization function C is defined as

$$C(s) = \int_{\mathbb{R}^d} \frac{2(1-\cos(\xi_1))}{\|\xi\|^{d+2s}} \frac{\mathrm{d}\xi}{(2\pi)^{d/2}} = \frac{\pi^{1/2}\Gamma(s+1/2)}{2^{d/2}s\Gamma(2s)\sin(\pi s)\Gamma(s+d/2)}.$$

Worth noting is that for a constant function $h(x) = H$ we obtain the ordinary fBf.

Proposition 2.4.3. *Let B_h be a multifractional Brownian motion (mBm for short) with multifractional function h. Then,*

$$\mathbb{E}\left[B_h(x)B_h(y)\right] = D(h(x),h(y))\left(\|x\|^{h(x)+h(y)} + \|y\|^{h(x)+h(y)} - \|x-y\|^{h(x)+h(y)}\right) \tag{2.11}$$

where

$$D(s,t) = \frac{\sqrt{\Gamma(2s+1)\Gamma(2t+1)\sin(\pi s)\sin(\pi t)}\Gamma(\frac{s+t+1}{2})}{2\Gamma(s+t+1)\sin(\pi(s+t))\Gamma(\frac{s+t+d}{2})},$$

for $t, s \in (0,1)$.

With the covariance function for a mBm defined we are now in a setting where it is possible to model simulations, this will be further explained in the next chapter.

Example 2.4.1. In Chapter 4 where we cover the numerical examples we will present a numerical study for different functions h and find the corresponding convergence order. This framework will be explained in Chapter 3. One of these functions is $h(t) = t$ defined on the one-dimensional domain $T = [0,1]$. This function together with a trajectory is presented in Figure 2.9. Next we also present these in the two-dimensional unit square with corresponding Hurst function $h(x,y) = x$, this is illustrated in Figure 2.10.

Now recall the functions ψ_λ from the Lemarié–Meyer basis (2.9).

Definition 2.4.6. For $\lambda \in \Lambda,\ x \in \mathbb{R},\ y \in (0,1)$ we define

$$\chi_\lambda(x,y) = \int_{\mathbb{R}} \frac{e^{-ix\xi} - 1}{|\xi|^{y+1/2}} \overline{\widehat{\psi}_\lambda(\xi)} \frac{\mathrm{d}\xi}{(2\pi)^{1/2}}.$$

Worth mentioning here is that we have seen this function before with set parameters in Theorem 2.3.1 for fractional Brownian motion, that is $\chi_\lambda(t,H) = \mathcal{I}_H(\psi_\lambda)$.

Theorem 2.4.1. *Let*

$$\widehat{W^+}(\mathrm{d}\xi) = \sum_{\lambda\in\Lambda} \overline{\widehat{\psi}_\lambda(\xi)}\eta_\lambda \,\mathrm{d}\xi$$

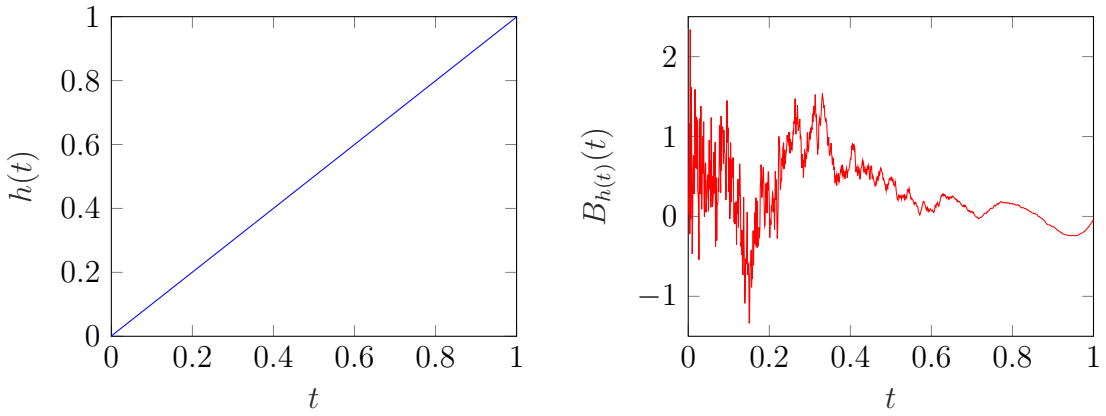

Figure 2.9: On the left is the function $h(t) = t$ in the domain and on the right is a generated sample path of the mBm with corresponding Hurst parameter to the function h

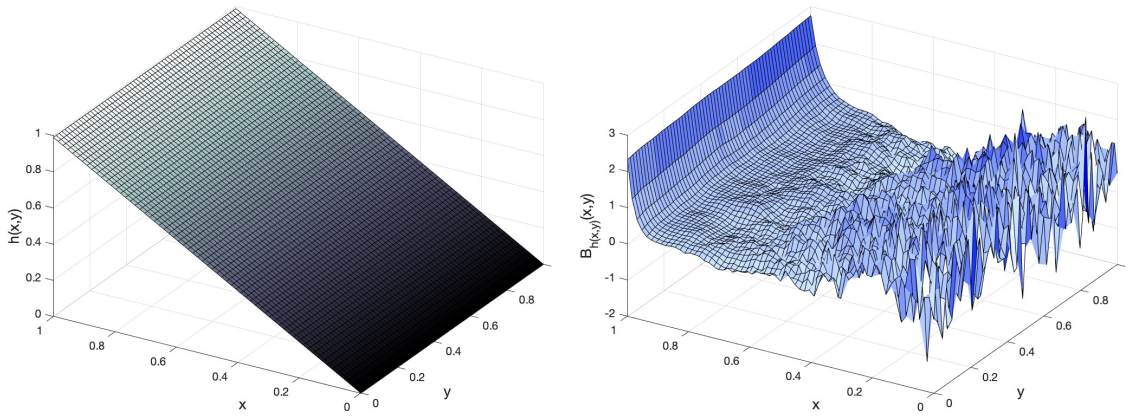

Figure 2.10: On the left is the function $h(x, y) = x$ in the domain and on the right is a generated sample path of the mBf B_h with corresponding Hurst parameter to the function h

be a Brownian random measure and the functions χ_λ defined as in Definition 2.4.6, then one gets the following series representation of the multifractional Brownian motion

$$B_h(t) = \frac{1}{(C(h(t)))^{1/2}} \sum_{\lambda \in \Lambda^+} \chi_\lambda(t, h(t)) \eta_\lambda.$$

This convergence is in $L^2(\Omega)$ and if h is locally Hölder continuous with exponent β, the series converges a.s. for the uniform convergence on compact interval.

Proposition 2.4.4. *Let $h : \mathbb{R}^d \to (0, 1)$ be a β-Hölder continuous multifractional function and B_h be the corresponding multifractional Brownian field. Next assume $\beta > \sup_{x \in \mathbb{R}^d} h(x)$, then*

$$\lim_{\varepsilon \to 0^+} \frac{\mathbb{E}\left[(B_h(x + \varepsilon u_1) - B_h(x + \varepsilon u_2))^2\right]}{\varepsilon^{2h(x)}} = \|u_1 - u_2\|^{2h(x)}$$

for all $u_1, u_2 \in \mathbb{R}^d$. Moreover the limit is uniform if $u_1, u_2 \in K$ for a compact space $K \subset \mathbb{R}^d$.

With these results we have now covered the random fields of interest and we are thus ready to go into the main part of this thesis, namely that of the approximation of the multifractional fields.

3

Approximation of multifractional Brownian fields

In order to numerically approximate the stochastic fields defined in chapter 2 we need to define a framework. To this end we will in this chapter cover how fractional and multifractional Brownian fields can be constructed in a way such that the convergence order of the scheme can be measured. We want to consider methods that can be implemented in a reasonable fashion, i.e. not focused on efficiency and instead a focus on generating fields with the correct distribution. First, to even consider methods that can be evaluated, we need to define the error we are measuring with respect to.

3.1 Convergence

This thesis mainly concerns the strong error which is a path-dependent error.

3.1.1 Strong error

The strong error compares sample-wise the field and its approximation. That is, we are trying to approximate the field $(X(t),\ t \in T)$ with $(X_h(t),\ t \in T_h)$ which depends on some discretization T_h where h usually refers to the largest discretization step.

Definition 3.1.1. For a stochastic field $(X(t),\ t \in T)$ in the space $L^2(\Omega; E)$ and a given numerical scheme depending on a discretization T_h, the numerical approximations $(X_h, h > 0)$ *converge strongly* to X if

$$\lim_{h \to 0} \mathbb{E}\left[\|X - X_h\|_E\right] = 0,$$

for a normed space $(E, \|\cdot\|)$. Next if it exists a $C > 0$ and $h_0 > 0$ s.t. for all $h \leq h_0$

$$\mathbb{E}\left[\|X - X_h\|_E\right] \leq Ch^\alpha,$$

then the numerical scheme *converges strongly with order* $\alpha > 0$.

In this study we will consider the space $L^2(\Omega; L^2(T; \mathbb{R}))$ with the following norm

$$\mathbb{E}\left[\|X - X_h\|^2_{L^2(T)}\right]^{1/2} = \mathbb{E}\left[\int_T |X(t) - X_h(t)|^2 \,\mathrm{d}t\right]^{1/2},$$

and the space $L^2(\Omega; C(T;\mathbb{R}))$ which has the following norm

$$\mathbb{E}\left[\|X - X_h\|^2_{L^\infty(T)}\right]^{1/2} = \mathbb{E}\left[\operatorname*{ess\,sup}_{t\in T} |X(t) - X_h(t)|^2\right]^{1/2}.$$

Note that these norms, which will define how we calculate the error of the scheme, depend on the exact continuous sample path $X(t)$ for all $t \in T$.

3.2 Simulation methods

Now with the errors defined we will explain how we aim to simulate the sample paths. In the literature one can find multiple methods of simulating fractional Brownian fields ([5], [12], [3]). The most important and difficult task with our approach is simulating the field such that the stationarity of the increments is kept. In this section some simulation methods will be mentioned and explained.

3.2.1 Random midpoint displacement

The first method considered is the random midpoint displacement method which can accurately generate a trajectory of a Brownian motion which is shown in Example 3.2.1. However, when one wants to construct the process with a fractional parameter, one loses the stationarity of the increments and hence this method is not ideal for the purposes of this thesis.

There is a new modification to this method called the conditionalized random midpoint displacement (RDM_{nm}) which was originally introduced in [16]. This method tries to lower the computational complexity and hence becomes a more viable option compared to the original method which is fairly computationally heavy. RDM is later explored in [5]. In this paper the author reaches the conclusion that this might be one of the better options for simulating fractional Brownian motion with regards to the time component. However it still lacks the property of producing stationary fields which is an essential problem. Even though this method might be useful in many cases, in this scenario where we want to do a convergence study with respect to the mesh it will not be of much use unfortunately.

Example 3.2.1. Let us recall example 2.1.1 of the ordinary Brownian motion on the domain of the unit interval. We will briefly demonstrate how one would use the random midpoint displacement to generate an accurate sample path of this process on $T = [0, 1]$. This is done similarly to [4].

Begin by setting $B(0) = 0$ and commence by generating $B(1)$ as a centered Gaussian random variable with variance 1. Next we construct the midpoint $B(1/2)$ by generating a Gaussian random variable with mean $B(1)/2$ and variance $1/2$. This procedure continues by constructing $B(1/4)$ as a Gaussian random variable with mean $B(1/2)/2$ and variance $1/4$. $B(3/4)$ is constructed similarly. This is iterated for 2^k nodes and the i:th node will be generated with mean $(B((i+1)/2^k) - B((i-1)/2^k))/2$ and variance 2^{-k}.

3.2.2 Cholesky method

The second procedure considered to simulate and numerically find convergence rates for fractional and multifractional Brownian fields are through a method using the Cholesky decomposition, henceforth this method will be called the Cholesky method.

This method consists in constructing a covariance matrix $(R_{i,j})_{i,j}$ which aims to approximate the covariance function $R(s,t) = \mathbb{E}[X(s)X(t)]$ for the centered Gaussian field X. To simulate the desired field with this approach we follow a few simple steps.

- First we consider a mesh of elements $\{M_i\}_{i\in I}$ in our domain $D \subset \mathbb{R}^d$.
- Next we construct the covariance matrix $R = (R(M_i, M_j)_{i,j\in I})$.
- Then we do a Cholesky decomposition of R into $R = LL^T$, where L is a lower triangular matrix. This is possible since R fulfills Proposition 2.1.2.
- Finally by simulating a standard normal random vector Z of dimension $|I|$ the field $X = LZ$ will have the desired covariance structure of R. This is enough since any Gaussian distribution is uniquely defined by its first two moments.

Computation-wise, the most heavy part of this procedure is the decomposition of the covariance matrix, this part can be shown to have a complexity of $O(N^3)$ [8]. The remaining part however, which is important as well for each simulation of the field, will have a numerical complexity of $O(N^2)$. Since we only need to evaluate the matrix L once for each discretization, the only remaining difficulty is how to handle the generated random numbers. This will be discussed closer in the next chapter. Assuming we are interested in a finite number of points this method is exact in the sense that we have no errors due to approximation of the distribution, but simply errors due to the discretization.

3.2.3 FieldSim

In [4] and [12] another method is introduced which is based on the two previous mentioned algorithms. This method is developed on the basis of the Cholesky method and the RMD method. This will be demonstrated by a more concrete example below, after the method is explained. The main idea is fairly simple. First one simulates the field with the Cholesky method in N_1 nodes of the domain. In the next step one uses a so-called fast step to simulate the field in the remaining $N_2 = N - N_1$ nodes, assuming one wants an accuracy of N nodes. Depending on the relation between N_1 and N_2 one can control the accuracy and computational time to some extent. For larger N_1 it takes on a higher accuracy for the price of a longer computational time.

Example 3.2.2. Let us assume we want to simulate a Gaussian process on $[0,1]$ with covariance function R. Then we decide we want to simulate the field X in $N = 10$ nodes of the domain, see Figure 3.1a. Next we pick N_1, e.g. 4, and do exactly the procedure described in the Cholesky method. Thus we have $X(t_i)$ for $t_i \in I_1 = \{0, \frac{1}{N_1-1}, \dots, 1\}$, see Figure 3.1b.

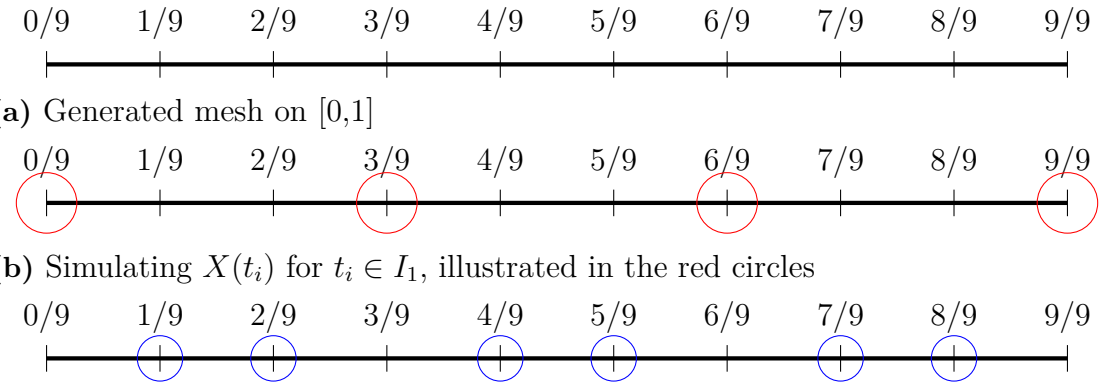

(a) Generated mesh on [0,1]

(b) Simulating $X(t_i)$ for $t_i \in I_1$, illustrated in the red circles

(c) Simulating $X(t_j)$ for $t_j \in I_2$ based on the closest nodes in $t_i \in I_1$. The $t_j \in I_2$ nodes are illustrated by the blue circles

Figure 3.1: Example of FieldSim procedure

Second step we want to simulate the remaining N_2 values of X, that is $X(t_i)$ for $t_i \in I_2 = \{\frac{1}{N-1}, \frac{2}{N-1}, \frac{4}{N-1}, \ldots, \frac{N-2}{N-1}\}$, see Figure 3.1c. Now this method consists of taking advantage of the already simulated values, which are assumed to be exact, and use the orthogonal projection, denoted $X_{\mathcal{X}_j}$ of those to approximate $X(t_j)$ for $t_j \in I_2$. This is done by simulating a Gaussian random variable with a specific variance, the details of this are explained in [12]. Finally we have simulated $(X(t_i),\ t_i \in I_1 \cup I_2)$, seen in Figure 3.2.

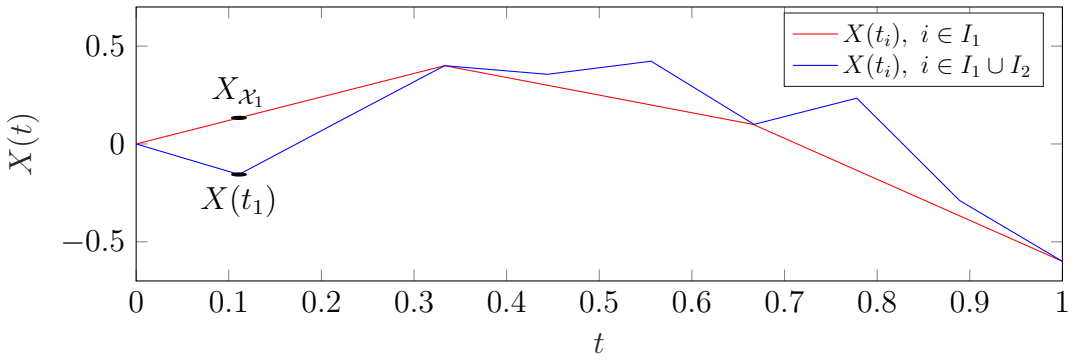

Figure 3.2: Generated Gaussian process from Example 3.2.2

One of the drawbacks of this simulation is just as in the previous method of the RMD we lose some accuracy in this second step and thus are only approximating the covariance R. The main disadvantage of this algorithm is with respect to the random numbers. It would be very technical, if possible, to use the same generated Gaussian random numbers when comparing two discretizations.

3.3 Implementation

These simulation techniques have different advantages and while the Cholesky approach is not the one with lowest numerical complexity it compensates with accuracy.

In this section we will describe how the previous examples of processes have been simulated and also how we evaluate the error introduced in Section 3.1. First, the different conditions for the mesh and dimensions will be considered. Second, the chosen method, the Cholesky method will be explained closer and how we aim to compare the errors between different mesh sizes.

3.3.1 Discretization

Recall the property of self-similarity in Definition 2.3.1 and that all the processes we are considering are either H-self-similar or lass. The processes on the domain $T = [0, 1] \subset \mathbb{R}$ will thus have the same distribution as in the whole domain of $\mathbb{R}$ up to a constant. This first assumption should not effect as much as the next, which is that of an equidistant mesh which will be the first to be considered.

Let V_k be the equidistant discretized mesh of Ω. To simplify even more, we will consider meshes of twice the distance between mesh points compared to the finer one. That is for the most coarse discretization $V_1 = V_{\frac{1}{N_0}}$ the distance between two mesh points is $\frac{1}{N_0}$ and for the second most coarse discretization the distance is $\frac{1}{2N_0}$. This procedure is repeated for K iterations.

$$\begin{aligned} V_1 = V_{\frac{1}{N_0}} &= \left\{0, \frac{1}{N_0}, \frac{2}{N_0}, \ldots, 1\right\}, \\ V_2 = V_{\frac{1}{2N_0}} &= \left\{0, \frac{1}{2N_0}, \frac{2}{2N_0}, \ldots, 1\right\}, \\ &\vdots \\ V_K = V_{\frac{1}{2^{K-1}N_0}} &= \left\{0, \frac{1}{2^{K-1}N_0}, \frac{2}{2^{K-1}N_0}, \ldots, 1\right\}. \end{aligned}$$

By this construction the discretizations will contain $|V_k| = \left|V_{\frac{1}{2^{k-1}N_0}}\right| = 2^{k-1}N_0 + 1$ mesh points. In the next part we will refer to each mesh point in V_k as $t_i^k = \frac{i}{2^{k-1}N_0}$

3.3.1.1 Adaptive mesh

In the next chapter we will show convergence results for different multifractional functions and in these cases there are functions that vary more in certain parts than others. For this reason it would be of interest to consider an adaptive mesh as well. For example concentrating more nodes close to neighbourhoods where $\left|\frac{\mathrm{d}h(x)}{\mathrm{d}x}\right|$ is large. One way of constructing such a mesh is in the following way: Assume

$$\int_0^1 \left|\frac{\mathrm{d}h(x)}{\mathrm{d}x}\right| \mathrm{d}x = C > 0$$

and define

$$\phi(x) = \frac{1}{C}\int_0^x \left|\frac{\mathrm{d}h(y)}{\mathrm{d}y}\right| \mathrm{d}y.$$

Next since ϕ is clearly continuous and $\phi(0) = 0$ and $\phi(1) = 1$ we can define points $\{x_i,\ i = 0, \dots, N\}$ s.t. $\phi(x_i) = \frac{i}{N}$. These points $\{x_i\}$ would be the mesh of a given size of $N+1$ mesh points. This way of constructing an adaptive mesh is done in [2].

3.3.2 Cholesky method simulation

Assuming the equidistant discretizations $V_1, \dots, V_K$, we want to evaluate the simulations, trajectories of the processes. This will be done in the following steps.

- Calculate the covariance matrix R given each discretization $V_1, \dots, V_K$:

$$R^k = \begin{bmatrix} R(t_0^k, t_0^k) & \dots & R(t_0^k, t_{2^{k-1}N_0}^k) \\ \vdots & \ddots & \vdots \\ R(t_{2^{k-1}N_0}^k, t_0^k) & \dots & R(t_{2^{k-1}N_0}^k, t_{2^{k-1}N_0}^k) \end{bmatrix}$$

  with the use of the chosen covariance function $R(s,t)$ belonging to the corresponding field $(X(t),\ t \in [0,1])$.

- Given every R^k we do the Cholesky decomposition into the lower triangular matrix L^k s.t. $LL^T = R$.

- Next we want to generate appropriate random numbers that should correspond to the same centered Gaussian vector Z. This is done with regard to the finest mesh first and then onto the coarser meshes. By first simulating a Gaussian random vector Z^K of length $2^{K-1}N_0 + 1$ and then summing up the values in the following way:

$$Z^K = \underbrace{\begin{pmatrix} Z_0 \\ Z_1 \\ \vdots \\ Z_{2^{K-1}N_0} \end{pmatrix}}_{(2^{K-1}N_0+1)\times 1} \text{ where } Z_i \sim \mathcal{N}(0,1),$$

$$Z^{K-1} = \frac{1}{\sqrt{2}} \underbrace{\begin{pmatrix} \sqrt{2}Z_0 \\ Z_1 + Z_2 \\ \vdots \\ Z_{2^{K-1}N_0-1} + Z_{2^{K-1}N_0} \end{pmatrix}}_{(2^{K-2}N_0+1)\times 1},$$

$$\vdots$$

$$Z^1 = \frac{1}{\sqrt{2^{K-1}}} \underbrace{\begin{pmatrix} \sqrt{2^{K-1}}Z_0 \\ \sum_{m=1}^{2^{K-1}} Z_m \\ \vdots \\ \sum_{m=2^{K-1}(N_0-1)+1}^{2^{K-1}N_0} Z_m \end{pmatrix}}_{(N_0+1)\times 1},$$

  then every random vector will have the desired $\mathcal{N}(0,1)$ distribution.

- Finally we have the desired approximated field $X^k = L^k Z^k$ for $k = 1, \dots, K$ with the covariance of R^k.

Next step is to evaluate the error between $X^k(t)$ and $X(t)$ with the use of interpolation.

3.3.3 Error analysis

Given the desired fields X^k from above we want to define exactly how each error is evaluated. Since we do not have the exact solution X we will use a reference solution, that is the finest approximated field X^K.

Now since the processes are generated upon different mesh sizes we need to do an interpolation for the more coarse processes such that they contain the same number of mesh points as the finest one. In this report we opt for ordinary linear interpolation:

$$X^k(t) = \left(1 - \frac{t - t_i}{t_{i+1} - t_i}\right) X^k(t_i) + \frac{t - t_i}{t_{i+1} - t_i} X^k(t_{i+1}),$$

for $t \in (t_i, t_{i+1}]$. Next with these new interpolated values every approximated process $\{X^1, \dots, X^K\}$ has values in $2^{K-1}N_0 + 1$ mesh points. To ease notation we define this variable as $N := 2^{K-1}N_0 + 1$, which is not to be confused with N_0 which is only the number of nodes in the coarsest discretization.

The next step is to simply calculate the error we are interested in. Recall from Section 3.1 where we defined the L^2- and L^∞-norms:

$$\mathbb{E}\left[\|X - X_h\|^2_{L^2(T)}\right]^{1/2} = \mathbb{E}\left[\int_T |X(t) - X_h(t)|^2 \,\mathrm{d}t\right]^{1/2},$$
$$\mathbb{E}\left[\|X - X_h\|^2_{L^\infty(T)}\right]^{1/2} = \mathbb{E}\left[\operatorname*{ess\,sup}_{t \in T} |X(t) - X_h(t)|^2\right]^{1/2}.$$

We approximate these inner norms in the following way for each simulation:

$$\|X - X_h\|^2_{L^2(T)} \approx \frac{1}{N-1} \sum_{n=1}^{N} \left|X^K(t_n) - X^k(t_n)\right|^2,$$
$$\|X - X_h\|^2_{L^\infty(T)} \approx \max_{t_n \in V^K} \left|X^K(t_n) - X^k(t_n)\right|^2.$$

3.3.4 Monte Carlo sampling

To evaluate these expectations numerically we do Monte Carlo samples, that is we approximate the expectation in the following way:

$$\mathbb{E}\left[\|X - X_h\|^2_{L^2(T)}\right]^{1/2} \approx \sqrt{\frac{1}{M} \sum_{m=1}^{M} \left\|X^{(m)} - X_h^{(m)}\right\|^2_{L^2(T)}},$$
$$\mathbb{E}\left[\|X - X_h\|^2_{L^\infty(T)}\right]^{1/2} \approx \sqrt{\frac{1}{M} \sum_{m=1}^{M} \left\|X^{(m)} - X_h^{(m)}\right\|^2_{L^\infty(T)}}$$

where $(X^{(m)}, m \in \mathbb{N})$ is a sequence of i.i.d. samples of the process X.

This together with the discretized approximation yields the following form:

$$\mathbb{E}\left[\|X - X_h\|^2_{L^2(T)}\right]^{1/2} \approx \sqrt{\frac{1}{M}\sum_{m=1}^{M}\frac{1}{N-1}\sum_{n=1}^{N}|X^{K,m}(t_n) - X^{k,m}(t_n)|^2},$$

$$\mathbb{E}\left[\|X - X_h\|^2_{L^\infty(T)}\right]^{1/2} \approx \sqrt{\frac{1}{M}\sum_{m=1}^{M}\max_{t_n \in V^K}|X^{K,m}(t_n) - X^{k,m}(t_n)|^2}.$$

Now it is important to note that we have two types of errors here, both a statistical one that is due to the Monte Carlo sampling which depends on M and a discretization which is because of the chosen step sizes h. Since we are investigating the strong error we are interested in controlling the statistical error and to let the discretization error be the critical one that we will measure. This is done by setting $M > h^{-2}$ for the finest $h^K = \frac{1}{N-1}$. Analysis behind Monte Carlo sampling of this kind can be found in [9] where it is covered in more detail.

3.3.5 Algorithm

This section will simply contain the algorithm to make the procedure clear how it is intended to work. Implementation-wise the Cholesky method was implemented into MATLAB which can be found in Appendix A, while the FieldSim algorithm is in open source *R*-code [3].

Algorithm 1: Cholesky Method

initialize K, M, N_0;
Error_{L^2} = zeros(K,1);
Error_{L^∞} = zeros(K,1);
for *k=1:K* **do**
  initialize V^k;
  calculate $R^k(V^k)$;
  Cholesky decompose $LL^T = R^k$;
end
for *m=1:M* **do**
  $Z^K = \text{randn}(0, 1)$;
  $X^K = L^K Z^K$;
  for *k=1:K-1* **do**
    $Z^k = \text{resum}(Z^K, 2^{k-1}N_0)$;
    $X^k = L^k Z^k$;
    $X^k = \text{interpolate}(X^k, 2^{K-1}N_0 + 1)$;
    $\text{Error}_{L^2}(k) = \text{Error}_{L^2}(k) + L^2\text{norm}(X^K - X^k)$;
    $\text{Error}_{L^\infty}(k) = \text{Error}_{L^\infty}(k) + L^\infty\text{norm}(X^K - X^k)$;
  end
end
$\text{Error}_{L^2} = \sqrt{\frac{1}{M}\text{Error}_{L^2}}$;
$\text{Error}_{L^\infty} = \sqrt{\frac{1}{M}\text{Error}_{L^\infty}}$;

4

Numerical results

In this chapter we reach the main interest of this report, namely the actual results of the implementation. First, we will examine the standard fractional Brownian motion from Corollary 2.3.1 and Example 2.3.2 before moving on to more unique processes which depend on some multifractional function.

The primary objective is to examine the convergence rate with regard to the discretization and how this might relate to different Hurst functions h. This is done by first illustrating the Hurst function h and in some cases also trajectories of different discretizations. However, focus will lie on the convergence order of the process and hence this will be calculated by fitting a linear polynomial to the error-vectors. In MATLAB this is calculated with the `polyfit` function. We will show loglog plots of some of the processes to demonstrate how the more general figures are constructed that illustrate multiple convergence orders. These results are generated by the Cholesky method which was introduced in Section 3.2.2. It is important to note that to the best of our knowledge we are not aware of any theoretical convergence orders for any of these processes and thus have nothing to compare to.

4.1 Fractional Brownian motion

Fractional Brownian motion was introduced in Chapter 2 where we mentioned some of its basic properties. However if we recall Example 2.3.2 we can observe the regularity which will become important when investigating convergence orders. The increments of the process are negatively correlated for $H < 0.5$ and they are positively correlated for $H > 0.5$. This can be observed in the trajectories from the example. Another important property that has been of interest for the research community is the long-range dependency [10]. This is conditioned on the following sum,

$$\sum_{n=1}^{\infty} \mathbb{E}\left[B_H(1)(B_H(n+1) - B_H(n))\right].$$

The process is said to exhibit long-range dependency if the sum does not converge. This is the case for fBm with $H > 0.5$. Next with the understanding of how these processes alter for different Hurst parameters we present in Figure 4.1 loglog plots of the two processes over a Monte Carlo sample. This is done with 6 different discretization sizes. We can see that the convergence rate is different for the two in both norms. Overall the error is smaller for the fBm with a Hurst parameter of 0.8.

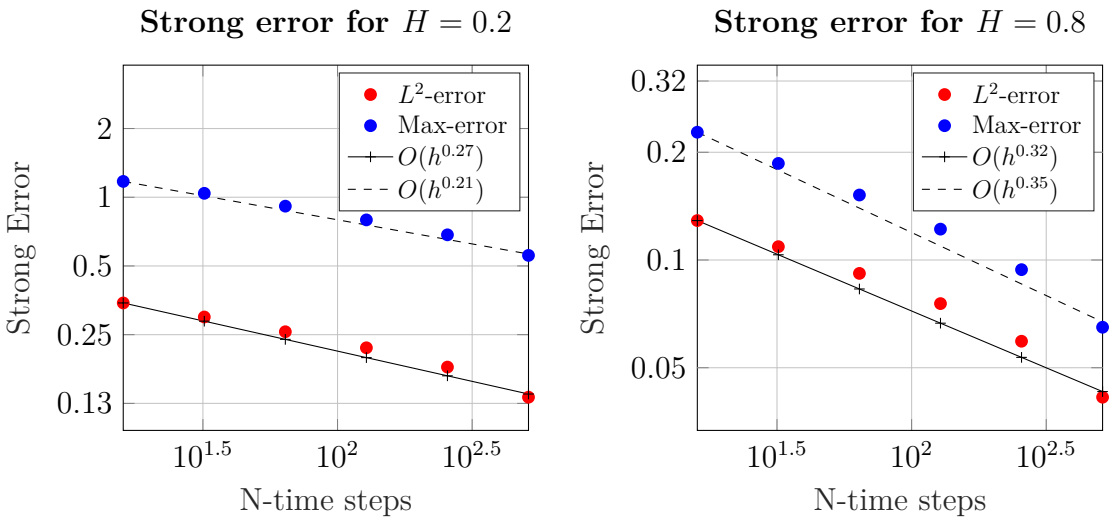

Figure 4.1: loglog-plots of the two errors for two fBm processes over increasing number of time steps N

Next we are interested in examining this for all $H \in (0, 1)$. In Figure 4.2 we illustrate the convergence orders for $H \in (0, 1)$. This is simulated with $N_0 = 16$, $K = 6$ and $M = 2N^2$. Clearly there is an almost linear dependency between the convergence order in both norms and the Hurst parameter on the interval $H \in (0, 0.6)$. However, after this interval we see that it goes down. Although the errors seem to become smaller (seen in Figure 4.1) we do not exhibit the same order of convergence.

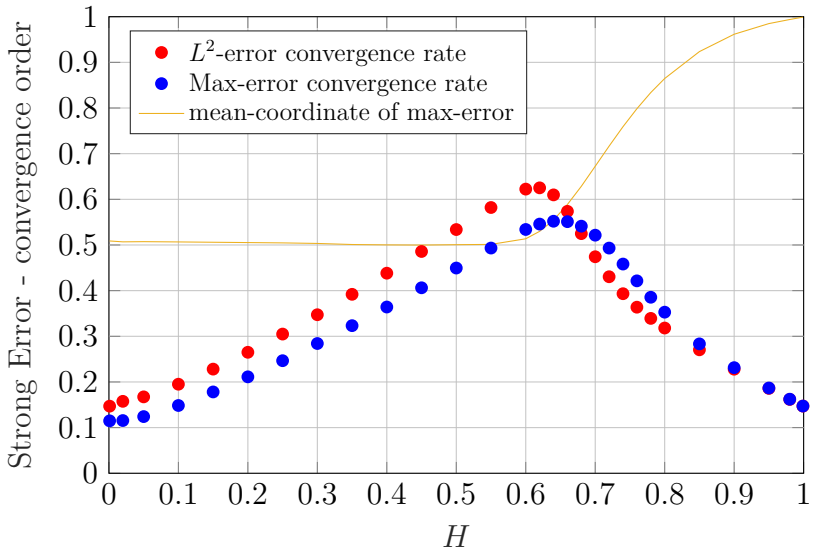

Figure 4.2: Convergence orders for fractional Brownian motion on the y-axis and the corresponding Hurst parameter H on the x-axis. Each tick corresponds to one convergence order for one fixed Hurst parameter. The y-axis also represents the domain $[0, 1]$ with regard to the mean-coordinate graph, this simply refers to where in the domain the maximal error occurs depending on which Hurst parameter that is in effect

4.2 Multifractional Brownian motion

The processes of interest in this section are different multifractional Brownian motions. That is, the aim is to examine the convergence order for different Hurst functions h that will vary over the domain $T = [0, 1]$. Functions of the following forms will be examined: increasing, decreasing, sinusoids and discontinuous functions.

4.2.1 Increasing Hurst functions

We will begin by examining mBm's with a strictly growing Hurst function. Recall Example 2.4.1 where we saw the Hurst function $h(t) = t$ and a generated path of this process. This function belongs to the first family of functions we examine.

4.2.1.1 Linear

Define functions of the form $h_Z(t) = Z + (1 - Z)t$. Each of these functions for every $Z \in (0, 1)$ is a function that will grow from Z up to 1 at the final time (or the right boundary) of the domain $T = [0, 1]$. In Figure 4.3 a few variations of this function are illustrated. It becomes evident that this last version $h_1(t) = 1$ is simply a fractional Brownian motion with Hurst parameter 1 and should yield the same convergence order as shown in the previous section.

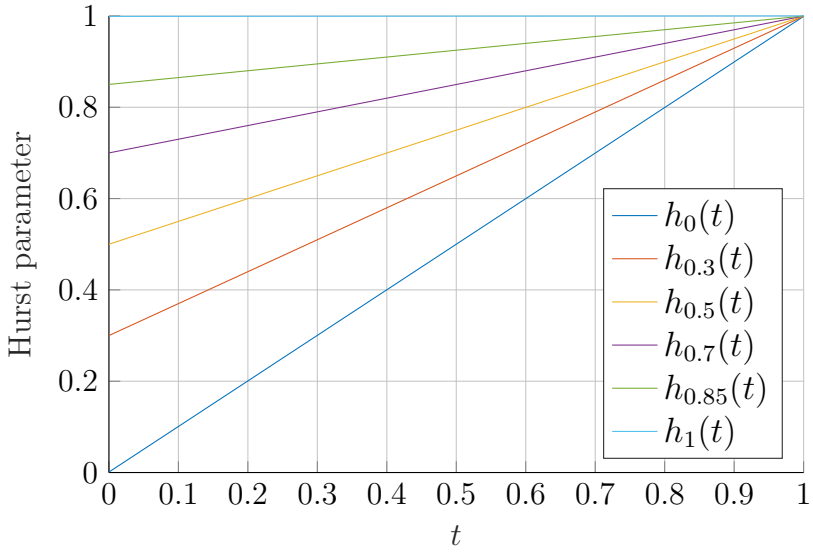

Figure 4.3: Six chosen examples of the functions $h_Z = Z + (1 - Z)t$ over the domain $[0, 1]$

These functions, particularly for small Z, start of with high oscillations and go on to become almost linear towards the end of the interval. This can be viewed in perspective of the Hausdorff dimension from (2.8) and Lemma 2.2.1, where the processes will exhibit a dimension of almost 2 at the beginning and dimension of 1 at the end. Recall the previous result in Figure 4.1 from fBm's where we found that

the error in both norms were larger for a smaller value of the Hurst parameter H. Based on that observation we would assume the errors for these processes would be greater in the left part of the domain given a small initial value of Z.

In Figure 4.4 the convergence order with regard to parameter Z is presented. There are a few interesting aspects to note here, especially compared to the orders of the ordinary fBm. First we can clearly observe the substantially higher convergence orders for parameter $Z \in [0.4, 0.7]$ in L^2 and $Z \in [0.4, 0.9]$ with regard to the max-norm. Secondly there is even more offset of the max-error curve from the L^2-error curve compared to the small offset for fBm's which can be observed in Figure 4.2. Finally we can confirm the fact that the maximal-error does on average occur early in the domain for values of $Z < 0.3$.

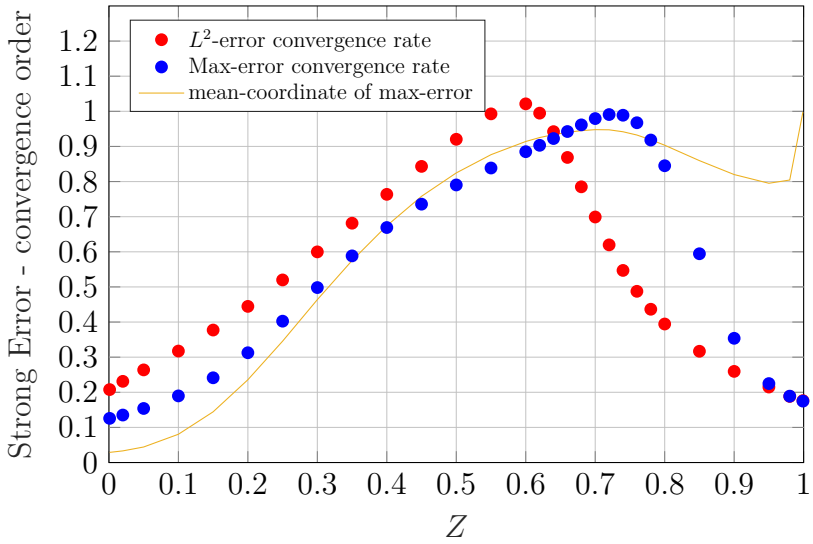

Figure 4.4: Convergence orders for the mBm defined by the Hurst functions $h_Z(t) = Z + (1 - Z)t$. The x-axis represent the parameter Z and the y-axis is the corresponding convergence order for the errors

4.2.1.2 Non-linear

The previous result did in some way increase mesh-dependency when the Hurst parameter linearly increased. The convergence order was higher when the process started with a Hurst parameter of Z and linearly increased to 1 compared to the ordinary fBm. Now a similar study is presented but for a function that increases in a non-linear fashion, $h_Z(t) = Z + (1 - Z)t^{1/4}$. In Figure 4.5 we present a few alterations of these Hurst functions.

Once again we measure the convergence order of the mBm's defined by this family of functions. This is illustrated in Figure 4.6 where we can observe even higher convergence orders than previously. So far these results have indicated that an increased mesh-dependency on h has yielded higher convergence orders.

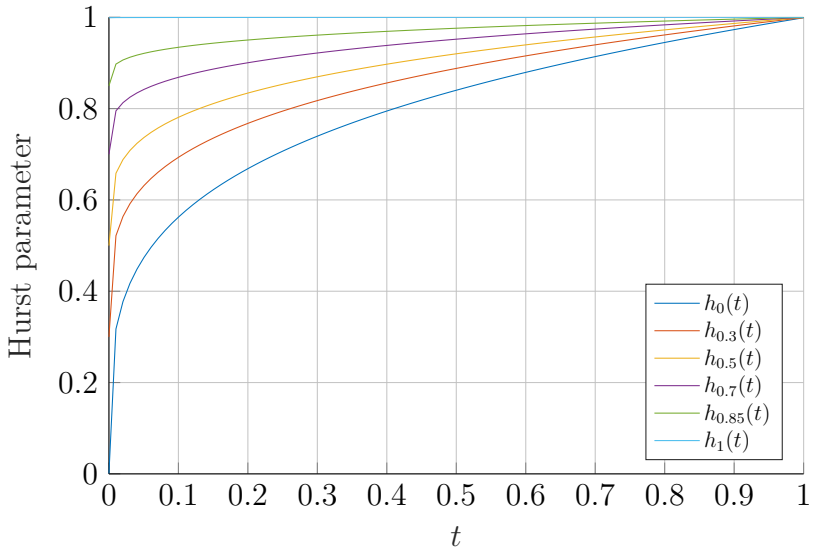

Figure 4.5: The graph of a subset of the family of Hurst functions defined on the form $h_Z(t) = Z + (1 - Z)t^{1/4}$ over the domain $[0, 1]$

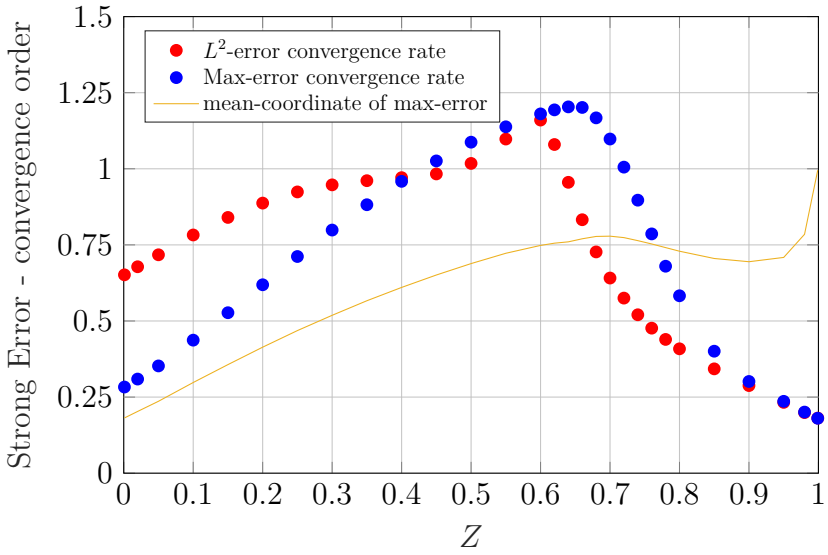

Figure 4.6: Convergence orders for the mBm defined by the functions $h_Z(t) = Z + (1 - Z)t^{1/4}$

4.2.2 Decreasing Hurst functions

We will now try to examine functions that are decreasing but also symmetric to our previous increasing functions. Consider the family of functions on the form $h_Z(t) = 1 - (1 - Z)t$ with $Z \in (0, 1)$. They are defined to all start in 1 and linearly decrease to Z over the domain $T = [0, 1]$. In Figure 4.7 we illustrate a few elements from this set of functions.

By construction these functions are symmetrical on the domain $[0, 1]$ in the $x = 0.5$ axis to the functions defined in 4.2.1.1. We are once again interested in evaluating the

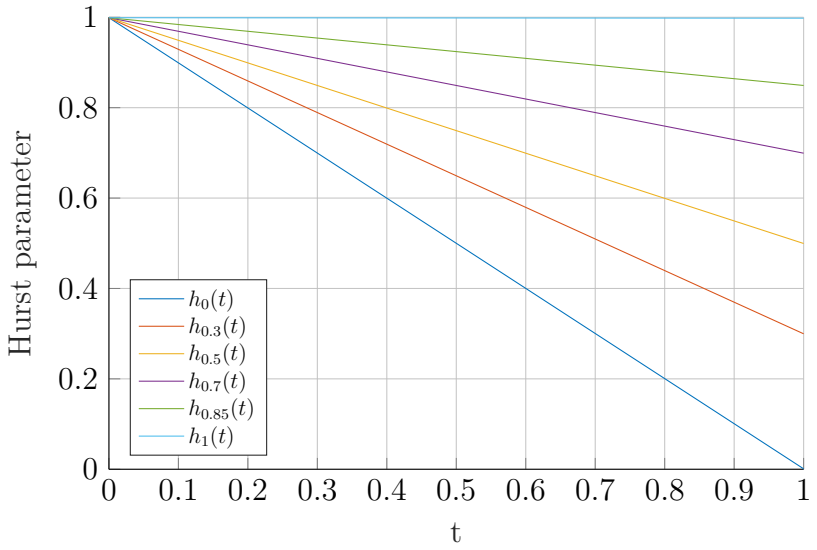

Figure 4.7: Illustration of some Hurst functions from the family of functions on the form $h_Z(t) = 1 - (1 - Z)t$

corresponding convergence orders. This is an indirect way of evaluating if ordinary norms, like the L^1- and L^2-norm, of h have a relation to the convergence order. That is, if this evaluation yields the same convergence order as previously we could suspect that this is the case. In Figure 4.8 the convergence orders are evaluated for each function corresponding to one value of $Z \in (0, 1)$. We can clearly see that this yields much lower convergence orders and as the functions become more flat and closer to the case of a fixed Hurst parameter $H = 1$ the order goes down.

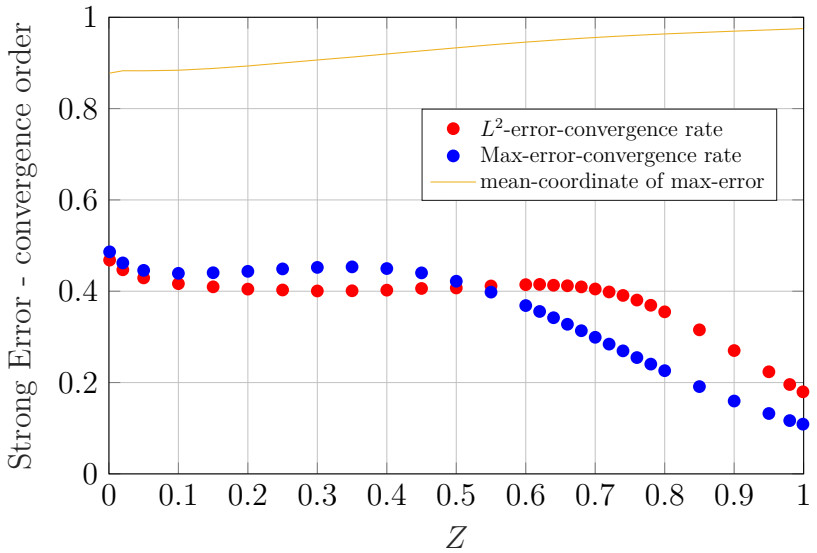

Figure 4.8: Convergence orders for the mBm defined by the Hurst function $h_Z(t) = 1 - (1 - Z)t$

4.2.3 Sinusoids

In this part we will cover a sinusoid function. That is a smooth function that varies over the domain in periods. We choose functions defined as

$$h_Z(t) = \begin{cases} Z + 0.8Z\sin(4\pi t) & Z \in (0, 1/2) \\ Z + 0.8(1-Z)\sin(4\pi t) & Z \in [1/2, 1), \end{cases}$$

with 2 periods in the domain $T = [0, 1]$. This family of functions is illustrated in Figure 4.9.

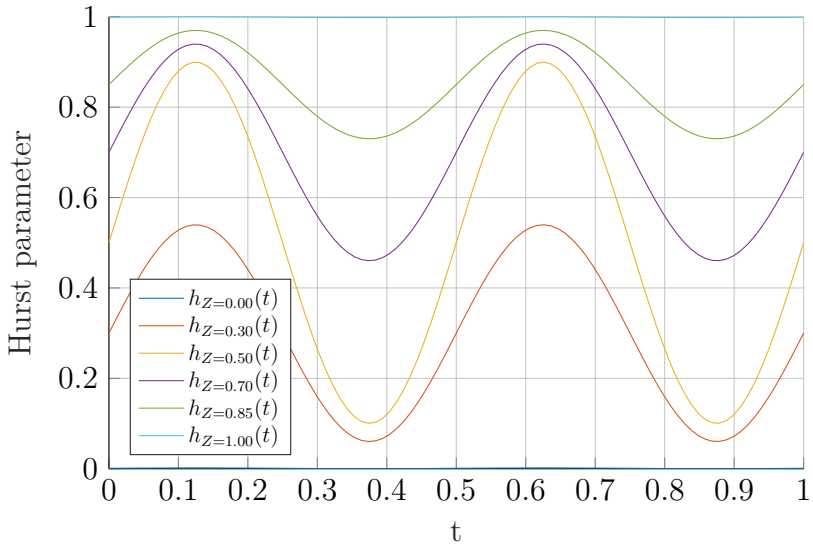

Figure 4.9: Illustration of a few chosen Hurst functions from the family of functions defined by $h_Z(t) = Z + 0.8Z\sin(4\pi t)$ for $Z \in (0, 1/2)$ and $h_Z(t) = Z + 0.8(1 - Z)\sin(4\pi t)$ for $Z \in [1/2, 1)$

To understand how these functions affect the mBm we illustrate in Figure 4.10 paths of mBm with respect to two values of Z.

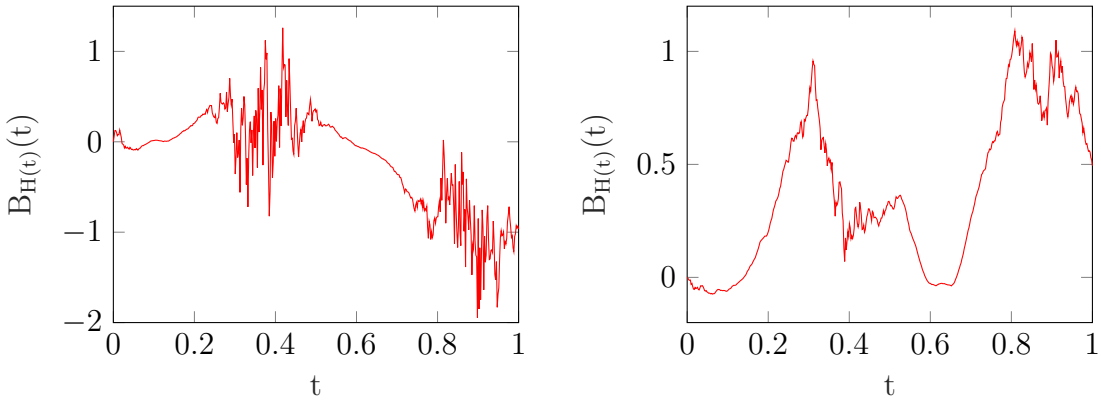

Figure 4.10: Paths of two mBm defined by the Hurst function $h_Z(t) = Z + 0.8(1 - Z)\sin(4\pi t)$ for $Z = 0.5$ to the left and $Z = 0.7$ to the right

Furthermore, a convergence study on these functions is shown in Figure 4.11. The orders are almost constant except for on the interval $(0.6, 0.8)$ where they are reaching a peak with regard to both norms. For $Z = 0.7$ this is the periodic function oscillating between 0.46 and 0.94 which yields convergence orders of about 0.75 in the L^2-norm and 0.5 in the Max-norm. This interval of values on the Hurst parameter could for example be compared to the strictly increasing function $h(t) = 0.5 + 0.5t$ illustrated in Figure 4.3. That process yields convergence orders in L^2-norm of 0.9 and in Max-norm of 0.8 which is clearly higher than for this process with a periodic Hurst function.

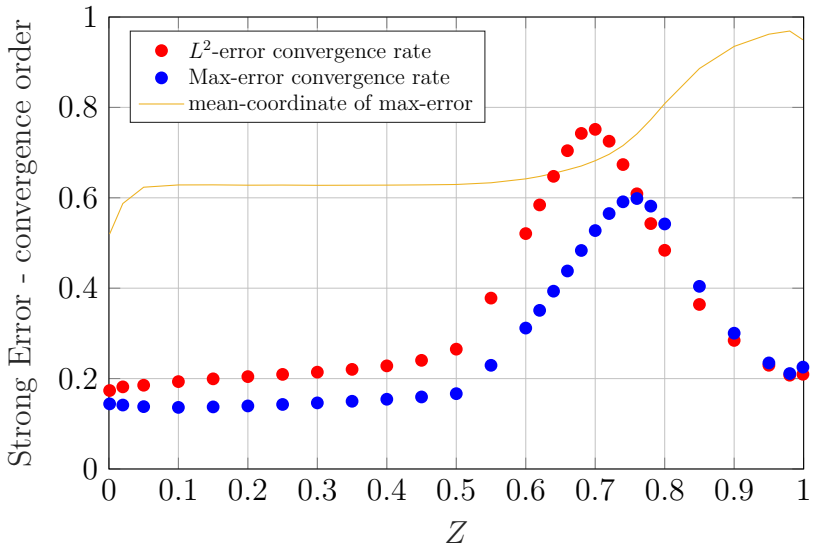

Figure 4.11: Convergence orders for the mBm defined by the Hurst function $h_Z(t) = Z + 0.8Z\sin(4\pi t)$ for $Z \in (0, 1/2)$ and $h_Z(t) = Z + 0.8(1 - Z)\sin(4\pi t)$ for $Z \in [1/2, 1)$

4.2.4 Discontinuous

In this section we will consider a discontinuous function to illustrate the role continuity plays with regard to the numerical approximation. Let the set of functions be defined in the following way

$$h_Z(t) = \begin{cases} 0.5 & t \in [0, Z) \\ 0.8 & t \in [Z, 1], \end{cases}$$

where $Z \in (0, 1)$. We illustrate these in Figure 4.12. This setting of course implies that when Z is close to 0 or 1 we are left with an ordinary fractional Brownian motion $B_H(t)$ for $H = 0.8$ and $H = 0.5$ respectively.

In the final convergence plot seen in Figure 4.13 we present the convergence orders for the discontinuous mBm. We can observe that the convergence orders here are very small and we would suspect large errors due to the jump.

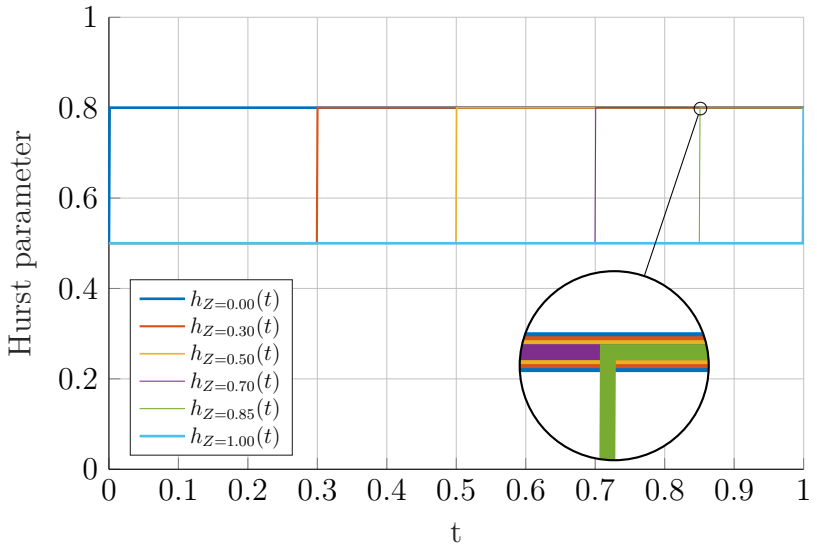

Figure 4.12: Illustration of a few chosen Hurst functions from the family of functions defined by $h_Z(t) = 0.5$ for $t \in [0, Z)$ and $h_Z(t) = 0.8$ for $t \in [Z, 1]$

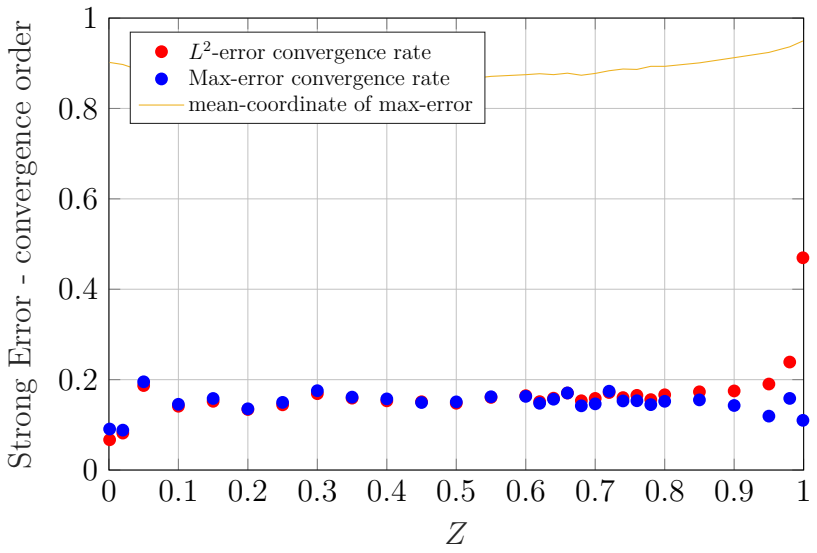

Figure 4.13: Convergence orders for the mBm defined by the Hurst function $h_Z(t) = 0.5$ for $t \in [0, Z)$ and $h_Z(t) = 0.8$ for $t \in [Z, 1]$

4.2.5 Discussion

Finally we are ready to summarize what has been accomplished and what remains for future work. We aimed at finding good ways to numerically simulate multifractional Gaussian processes. Further we wanted to measure how well we could simulate these processes. This thesis manages to numerically approximate fractional and multifractional Brownian motion. The primarily result concerns the convergence order for the fractional Brownian motion. With the Cholesky method we find that the convergence order in L^2 is strictly greater than the Hurst parameter in the

interval of $[0, 0.6]$ and might suggest a linear dependency between the two. After this interval we start to lose convergence rate, and in this thesis we do not manage to answer why that is. Something that is observed and not fully shown is that trajectories in the interval of $[0.7, 1]$ have a strange behaviour where it does not appear that they always converge with the current implementation. This is mostly speculations and should not be viewed as more than potential research directions for the future.

Next we did experiments with a number of different Hurst functions to find different properties. The main interest being of course how the convergence rate relates to the Hurst function of a multifractional Brownian motion. What was interesting to note is how the convergence rate was clearly above that of a fractional Brownian motion for a few different Hurst functions. Especially some of those that were strictly growing functions did exhibit a much higher convergence rate, some were above order one.

Something that was interesting to see as well was that we observed how the convergence rate depends on if the function was increasing or decreasing. This was done to see if we could find a relation between the Hurst function and the convergence order. More specifically if a Hurst function symmetrical to another function would yield the same convergence order. We could see that this was not the case and the decreasing functions exhibited lower convergence orders.

To the best of our knowledge there are no theoretical results available regarding the relation between the convergence order and the Hurst function. It now remains for future work to theoretically confirm the obtained results. Furthermore, it would be interesting to find a mathematical relation between the Hurst function and the order of convergence.

Bibliography

[1] Adler, R. J. and Taylor, J. E. (2007). *Random Fields and Geometry*. Berlin: Springer.

[2] Brenner, S. C. and Scott, L. R. (2008) *The Mathematical Theory of Finite Element Methods*, 3rd edn. Berlin: Springer.

[3] Brouste, A. and Lambert-Lacroix, S. (2015). FieldSim: Random Fields (and Bridges) Simulations. R package version 2.0.0. https://cran.r-project.org/web/packages/FieldSim/FieldSim.pdf

[4] Cohen, S. and Istas, J. (2013) *Fractional Fields and Applications*. Berlin: Springer.

[5] Dieker, A. B. (2002) *Simulation of fractional Brownian motion*, Master's thesis. Amsterdam: Vrije Universiteit Amsterdam. See http://www.columbia.edu/ ad3217/fbm.html.

[6] Falconer, K.J. (1992) *Fractal Geometry - Mathematical Foundations and Applications*. Chichester: John Wiley.

[7] Folland, G.B. (1992) *Fourier analysis and its applications*. Pacific Grove, California: Wadsworth & Brooks/Cole Advanced Books & Software.

[8] van de Geijn, R. A. (2014). *Notes on Cholesky Factorization*. Retrieved from The University of Texas on (28/1-2020): http://www.cs.utexas.edu/users/flame/Notes/NotesOnChol.pdf

[9] Gobet, E. (2016). *Monte-Carlo Methods and Stochastic Processes: From Linear to Non-linear*. Boca Raton, FL: CRC Press.

[10] Graves, T., Gramacy, R., Watkins, N. and Franzke, C. (2016) A Brief History of Long Memory: Hurst, Mandelbrot and the Road to ARFIMA, 1951–1980. *Entropy*, 19(9), 437.

[11] Karatzasand, I. and Shreve, S. (1988) *Brownian Motion and Stochastic Calculus*. Berlin: Springer.

[12] Lambert-Lacroix, S., Istas, J. and Brouste, A. (2007). On Fractional Gaussian Random Fields Simulations. *Journal of Statistical Software*. 23(1). pp. 1-23.

[13] Mandelbrot, B. and van Ness, J.W. (1968). Fractional Brownian motions, frac-

tional noises and applications. *SIAM Review*, 10 (4), pp. 422–437.

[14] Mandelbrot, B. (1983). *The Fractal Geometry of Nature*. San Francisco: W.H. Freeman.

[15] Mandelbrot, Benoit B. (1997). *Fractals and Scaling in Finance: Discontinuity, Concentration, Risk*. Berlin:Springer.

[16] Norros, I., Mannersalo, P. and Wang, J. (1999). Simulation of Fractional Brownian Motion with Conditionalized Random Midpoint Displacement. *Advances in Performance Analysis*, 2, pp.77-101.

[17] Stojic, T., Reljin, I. and Reljin, B. (2006). Adaptation of multifractal analysis to segmentation of microcalcifications in digital mammograms. *Physica A: Statistical Mechanics and its Applications*, 367, pp. 494–508.

A

Appendix

A.1 Matlab code

In this appendix we have the MATLAB code which implements the Cholesky method. It begins by evaluating the covariance matrix with the corresponding help functions. These help functions can be found after the initial code. Next it evaluates sample paths and calculating the corresponding error between the reference solution and the approximation.

MATLAB code

```
X = 1;                      % length of domain
eps = 10^(-32);             % small value
K = 6;                      % number of discretizations
dim = 1;                    % choose between dimension 1 and 2
Hurst = 0.6;

count = zeros(length(Hurst),1);
index_of_error = zeros(length(Hurst),1);

N_vector = zeros(K,1);  % will contain number of time steps
   in each discretization
N_vector(1) = 16;       % number of time steps in the most
   coarse discretization
for i=1:K-1
    N_vector(i+1) = 2*N_vector(i);
end


error_L2 = zeros(K,1);
error_max = zeros(K,1);


% mesh for the reference solution
N_finest = 2*N_vector(end);
mesh_finest = zeros(N_finest+1,1);
for i=1:N_finest+1
    mesh_finest(i) = eps+X*(i-1)/(N_finest);
end
```

```
27
28 % capital Z in the thesis, defining the parameter for the
      hurst function H below, set to a constant for a
      fractional Brownian motion
29 z = 0.6;
30 H = @(x)(z+0.999*(1-z)*x);
31 % use help function covMat_mbm with corresponding Hurst
      function H, mesh and dimension
32 [cov_finest,R_finest] = covMat_mBm(H,mesh_finest,dim);
33
34
35
36
37
38
39 % calculate the discretized meshes as well as their
      corresponding covariance matrix R and lower triangular
      matrix cov w.r.t. to given parameters
40
41 mesh = cell(K, 1);
42 cov = cell(K, 1);
43 R = cell(K, 1);
44
45 for k=1:K
46     N = N_vector(k);
47     mesh{k} = zeros(N+1,1);
48     for i=1:N+1
49         mesh{k}(i) = eps+X*(i-1)/(N);
50     end
51     [cov{k},R{k}] = covMat_mBm(H,mesh{k},dim);
52 end
53
54 % number of Monte Carlo samples
55 M = N_vector(end)^2;
56 for j=1:M
57     % generating the Gaussian random vector
58     Z_finest = randn((N_finest+1),1);
59     % evaluating the sample path
60     BM_finest = cov_finest*Z_finest;
61
62
63     for k=1:K
64         % evaluating the sample paths for the more coarse
              discretizations by summarizing the random
              numbers accordingly
65         N = N_vector(k);
66         l = N_finest/N;
67         Z = zeros(N+1,1);
68         for m=1:N
```

```
            for p=1:l
                Z(1+m) = Z(1+m) +
                   Z_finest(1+(m-1)*l+p)/sqrt(l);
            end
        end
        Z(1) = Z_finest(1);

        BM = cov{k}*Z;

        % calling the help function norm_LERP to evaluate
           the max-error "e_max" and the L2-error "e_L2"
        % also returning ind_x which contains the
           coordinate of where the max-error occurs
        [e_max , ind_x, e_L2] =
           maxnorm_LERP(BM_finest(2:end),BM(2:end),dim);

        error_L2(k) = error_L2(k)+e_L2;
        error_max(k) = error_max(k)+e_max;

        index_of_error = index_of_error + ind_x;


    end
end

% taking the sample mean for each discretization
for k=1:K
    error_L2(k) = error_L2(k)/M;
    error_max(k) = error_max(k)/M;
end

% convergence order
h_L2 = polyfit(log(N_vector),log(sqrt(error_L2)),1);
h_max = polyfit(log(N_vector),log(sqrt(error_max)),1);

% A function evaluating the covariance matrix R with a
   given Hurst function
% H. Returns this matrix as well as the lower triangular
   matrix L from
% doing a cholesky decomposition. Calling the help function
   cov_fBm which
% evalutes the covariance of the Gaussian field desired.
function [L,R] = covMat_mBm(H,mesh,dim)

if (dim == 1)
    N = length(mesh) -1;
    cov = zeros(N+1,N+1);
    for i=1:N+1
        H_x = H(mesh(i));
```

```
111         for j=1:i
112            H_y = H((mesh(j)));
113            cov(i,j) = cov_fBm(mesh(i),mesh(j),H_x,H_y,dim);
114            cov(j,i) = cov(i,j);
115         end
116     end
117     L = chol(cov,'lower');
118     R = cov;
119 end
120
121 if (dim == 2)
122     N = length(mesh);
123
124     for i=1:N
125         H_x = H(mesh(1,i),mesh(2,i));
126         for j=1:i
127            H_y = H(mesh(1,j),mesh(2,j));
128            cov(i,j) =
                  cov_fBm(mesh(:,i),mesh(:,j),H_x,H_y,dim);
129            cov(j,i) = cov(i,j);
130         end
131     end
132     L = chol(cov,'lower');
133     R = cov;
134 end
135 end
136
137 % A function taking in the values of the Hurst function in
       the desired
138 % coordinates as well as the coordinates and the dimension
       of the domain.
139 % It returns the covariance.
140
141 function [cov,D_h] = cov_fBm(x,y,H_x,H_y,dim)
142 if (dim == 1)
143     C_h = @(h)(pi^(1/2+1/2)*gamma(h+1/2)/(h*sin(pi*h)...
144                 *gamma(2*h)*gamma(h+1/2)))^(1/2);
145
146     D_h = C_h((H_x+H_y)/2)^2 /(2*(C_h(H_x))*(C_h(H_y)));
147
148     cov = D_h * (abs(x)^(H_x+H_y)+abs(y)^(H_x+H_y)-...
149                     abs(x-y)^(H_x+H_y));
150 end
151 if (dim == 2)
152     C_h = @(h)(pi^(dim/2+1/2)*gamma(h+1/2)/(h*sin(pi*h)...
153                 *gamma(2*h)*gamma(h+dim/2)))^(1/2);
154
155     D_h = (C_h((H_x+H_y)/2))^2 /(2*(C_h(H_x))*(C_h(H_y)));
156
```

```
157     cov = D_h * ((sqrt(x(1)^2 +
            x(2)^2))^(H_x+H_y)+(sqrt(y(1)^2 +
            y(2)^2))^(H_x+H_y)...
158           -(sqrt((x(1)-y(1))^2 + (x(2)-y(2))^2))^(H_x+H_y));
159 end
160
161 end
162
163 %% Assuming input is of size (n+1,1)
164 % Uses a linear interpolation on the form (1-j/N)*X_i + j/N
        * X_(i+1) for
165 % nodes lieing between X_i and X_(i+1). Evalutes the max
        error and L2 error
166 % between the two vectors. Also returns the average
        coordinate of where the
167 % maximal error occurs.
168
169
170 function [val_max, ind_x, val_mean] =
        maxnorm_LERP(BM1,BM2,dim)
171
172 if dim == 1
173     N1 = length(BM1);
174     N2 = length(BM2);
175
176     if (N1 == N2)
177         l = 1;
178         k = 0;
179     else if (N1 > N2)
180             l = (N1)/(N2);
181             k = 1;
182         else if (N1 < N2)
183                 l = (N2)/(N1);
184                 k = 2;
185             end
186         end
187     end
188     e = 0;
189     if k == 0
190         e = (abs(BM1 - BM2).^2);
191         [val_max,ind_x] = max(e);
192         val_mean = mean(e);
193     end
194
195     if k == 1
196         e = size(N1+1,1);
197         BM2 = [0 ; BM2];
198         BM1 = [0 ; BM1];
199         for i=1:N1
```

```
200             j = floor((i-1)/l)+1;
201             intpol =
                   BM2(j)*(j-(i-1)/l)+BM2(j+1)*((i-1)/l-j+1);
202             e(i) = abs(BM1(i)-intpol)^2;
203
204         end
205         e(N1+1) = abs(BM1(end)-BM2(end)).^2;
206         [val_max,ind_x] = max(e);
207         val_mean = mean(e);
208     end
209
210     if k == 2
211         e = size(N2+1,1);
212         BM1 = [0; BM1];
213         BM2 = [0 ; BM2];
214         for i=1:N2
215             j = floor((i-1)/l)+1;
216             intpol =
                   BM1(j)*(j-(i-1)/l)+BM1(j+1)*((i-1)/l-j+1);
217             e(i) = abs(BM2(i)-intpol)^2;
218         end
219         e(N2+1) = abs(BM1(end)-BM2(end))^2;
220         err = max(e);
221         [val_max,ind_x] = max(e);
222         val_mean = mean(e);
223     end
224
225     ind_x = ind_x/max(N1+1,N2+1);
226 end
227
228 if dim == 2
229     N1 = sqrt(length(BM1))-1;
230     N2 = sqrt(length(BM2))-1;
231
232     if (N1 == N2)
233         l = 1;
234         k = 0;
235     else if (N1 > N2)
236             l = (N1)/(N2);
237             k = 1;
238         else if (N1 < N2)
239                 l = (N2)/(N1);
240                 k = 2;
241             end
242         end
243     end
244
245     if k == 0
246         e = (abs(BM1 - BM2).^2);
```

```
247         val_max = max(e);
248         val_mean = max(e);
249     end
250
251     if k == 1
252         e = zeros((N1+1)*(N1+1),1);
253         en = zeros((N1+1)*(N1+1),1);
254
255         % Calculating the rows where we use a linear
               interpolation between
256         % two points
257         for row=1:N2+1
258             for col=1:N2
259                 for j=1:l
260                     intpol =
                           BM2((N2+1)*(row-1)+col)*(1-(j-1)/l)
                           + ...
261                         BM2((N2+1)*(row-1)+col+1)*((j-1)/l);
262                     e(l*(row-1)*(N1+1)+(col-1)*l+j) = ...
263                         abs(BM1(l*(row-1)*(N1+1)+...
264                         (col-1)*l+j)-intpol)^2;
265                 end
266             end
267             e(l*(row-1)*(N1+1)+N1+1) = ...
268                 abs(BM1(l*(row-1)*(N1+1)+N1+1)-...
269                 BM2((N2+1)*(row-1)+N2+1))^2;
270         end
271         % Calculating the columns where we use a linear
               interpolation
272         % between two points
273         for col=1:N2+1
274             for row=1:N2
275                 for j=1:l
276                     intpol =
                           BM2((row-1)*(N2+1)+col)*(1-(j-1)/l)
                           + ...
277                         BM2((row)*(N2+1)+col)*((j-1)/l);
278                     e(l*(row-1)*(N1+1)+1+...
279                     (col-1)*l+(j-1)*(N1+1)) = ...
280                         abs(BM1(l*(row-1)*(N1+1)+1+...
281                         (col-1)*l+(j-1)*(N1+1))-intpol)^2;
282
283                 end
284             end
285         end
286
287         % Calculating the remaing "inner points", that is
               mesh-nodes that
288         % doesn't have any row or column that interferes
```

```
            with the rougher
289         % mesh, and hence we will do a weighted linear
               interpolation
290         % between 4 mesh-points.
291
292         for row=1:N2
293             for col=1:N2
294                 for j=l-1
295                     for i=l-1
296             intpol
                   =(1-i/l)*(1-j/l)*BM2((row-1)*(N2+1)+col)+...
297                 (i/l)*(1-j/l)*BM2((row-1)*(N2+1)+col+1)+...
298                 (1-i/l)*(j/l)*BM2(row*(N2+1)+col)+...
299                 (i/l)*(j/l)*BM2(row*(N2+1)+col+1);
300
301             e(i+(j-1)*(N1+1)+(row-1)*l*(N1+1)+...
302             (col-1)*l+1+N1+1) = abs(BM1(i+(j-1)*(N1+1)...
303             +(row-1)*l*(N1+1)+(col-1)*l+1+N1+1)-intpol)^2;
304                     end
305                 end
306             end
307         end
308         val_max = max(e);
309         val_mean = mean(e);
310
311     end
312     if k == 2
313         e = zeros((N2+1)*(N2+1),1);
314         en = zeros((N2+1)*(N2+1),1);
315
316         % Calculating the rows where we use a linear
               interpolation between
317         % two points
318         for row=1:N1+1
319             for col=1:N1
320                 for j=1:l
321                     intpol =
                           BM1((N1+1)*(row-1)+col)*(1-(j-1)/l)...
322                         + BM1((N1+1)*(row-1)+col+1)*...
323                         ((j-1)/l);
324                 e(l*(row-1)*(N2+1)+(col-1)*l+j) = ...
325                     abs(BM2(l*(row-1)*(N2+1)+...
326                     (col-1)*l+j)-intpol)^2;
327                 end
328             end
329             e(l*(row-1)*(N2+1)+N2+1) =
                   abs(BM2(l*(row-1)*(N2+1)+N2+1)-...
330                 BM1((N1+1)*(row-1)+N1+1))^2;
331         end
```

```
332         % Calculating the columns where we use a linear
               interpolation
333         % between two points
334         for col=1:N1+1
335             for row=1:N1
336                 for j=1:l
337                     intpol =
                           BM1((row-1)*(N1+1)+col)*(1-(j-1)/l)
                           ...
338                         + BM1((row)*(N1+1)+col)*((j-1)/l);
339                     e(l*(row-1)*(N2+1)+1+(col-1)*l+...
340                     (j-1)*(N2+1)) =
                           abs(BM2(l*(row-1)*(N2+1)...
341                     +1+(col-1)*l+(j-1)*(N2+1))-intpol)^2;
342                 end
343             end
344         end
345
346         % Calculating the remaing "inner points", that is
               mesh-nodes that
347         % doesn't have any row or column that interferes
               with the rougher
348         % mesh, and hence we will do a weighted linear
               interpolation
349         % between 4 mesh-points.
350
351         for row=1:N1
352             for col=1:N1
353                 for j=l-1
354                     for i=l-1
355             intpol =
                   (1-i/l)*(1-j/l)*BM1((row-1)*(N1+1)+col)+...
356                  (i/l)*(1-j/l)*BM1((row-1)*(N1+1)+col+1)+...
357                  (1-i/l)*(j/l)*BM1(row*(N1+1)+col)+...
358                  (i/l)*(j/l)*BM1(row*(N1+1)+col+1);
359
360             e(i+(j-1)*(N2+1)+(row-1)*l*(N2+1)+(col-1)*l+1...
361             +N2+1) = abs(BM2(i+(j-1)*(N2+1)+...
362             (row-1)*l*(N2+1)+(col-1)*l+1+N2+1)-intpol)^2;
363                     end
364                 end
365             end
366         end
367         val_max = max(e);
368         val_mean = mean(e);
369     end
370     ind_x=1;
371 end
372 end
```